THE EFFECT OF WALL GAP ON DIELECTRIC MEASUREMENT FROM COAXIAL-CIRCULAR CELL

BY

SALAH MOHAMMED AL-OFI

A Thesis Presented to the
DEANSHIP OF GRADUATE STUDIES

KING FAHD UNIVERSITY OF PETROLEUM & MINERALS
DHAHRAN, SAUDI ARABIA

In Partial Fulfillment of the
Requirements for the Degree of

MASTER OF SCIENCE

In

ELECTRICAL ENGINEERING

MAY 2015

KING FAHD UNIVERSITY OF PETROLEUM & MINERALS

DHAHRAN- 31261, SAUDI ARABIA

DEANSHIP OF GRADUATE STUDIES

This thesis, written by Salah Mohammed Al-Ofi under the direction his thesis advisor and approved by his thesis committee, has been presented and accepted by the Dean of Graduate Studies, in partial fulfillment of the requirements for the degree of **MASTER OF SCIENCE IN ELECTRICAL ENGINEERING.**

Dr. Essam F. Hassan
(Advisor)

Dr. Ali A. Al-Shaikhi
Department Chairman

Dr. Hussain Al-Jamid
(Member)

Dr. Salam A. Zummo
Dean of Graduate Studies

Dr. Khurram K. Qureshi
(Member)

1/6/15
Date

عمادة الدراسات العليا
DEANSHIP OF GRADUATE STUDIES

I dedicate this work to my mother who always prays for me and to my wife and son who always give me support and inspiration to do the best out of me

ACKNOWLEDGMENTS

I would like to thank my managers at Schlumberger Dhahran Carbonate Research Center (SDCR), Dr. Mohammed Badri and Dr. Wael Abdallah who supported me to continue my Master degree. Also, I would like to thank my advisor at KFUPM Dr. Essam Hassan for his fruitful discussions and positive feedbacks that pushed my limits and made this work successful. I thank my technical advisor Dr. Reza Taherian from SDCR and Dr. Tarek Habashy for their technical discussion and critical review of the work. My gratitude goes also to SDCR lab technician Aslan Keskin who did an excellent job in the preparation of samples.

TABLE OF CONTENTS

LIST OF FIGURES

LIST OF ABBREVIATIONS

RF	:	Radio Frequency
TEM	:	Transverse Electromagnetic
TM	:	Transverse Magnetic
PEC	:	Perfect Electric Conductor
ODE	:	Ordinary Differential Equation
VNA	:	Vector Network Analyzer
SNR	:	Signal to Noise Ratio

ABSTRACT

Full Name : Salah Mohammed Al-Ofi

Thesis Title : The Effect of Wall Gap on Dielectric Measurement from Coaxial-Circular Cell

Major Field : Electromagnetics

Date of Degree : May 2015

We analyze the error caused by having a thin layer of dielectric material surrounding a cylindrical rock sample in a Coaxial-Circular measurement cell. We develop a full-wave model that can predict the fields inside the cell and predict the reflection coefficient from the coaxial circular junction. Galerkin's approach has been used to determine the electromagnetic fields in different parts of the cell by utilizing the boundary value problem. The sample complex dielectric permittivity has been determined by inverting the reflection coefficient (S_{11} parameter) data obtained using a network analyzer in the frequency range of 1MHz-500MHz. Furthermore, the reflection coefficient resulting from the analytical model is compared with COMSOL simulation for a known lossless and a lossy dielectric thin layer. Lab measurement on rock sample exhibiting wall gap is conducted and we found good match with our predicted S_{11} from our model.

ملخص الرسالة

الاسم الكامل: صلاح محمد العوفي

عنوان الرسالة: تأثير فجوة الجدار على قياس ثابت العازل الكهربائي بواسطة الموجِّه الموجي الدائري المحوري

التخصص: كهرومغناطيسية

تاريخ الدرجة العلمية: مايو 2015

في هذه الرسالة، نقوم بتحليل تأثير الفجوة الواقعة بين جدار الموجِّه الموجي الدائري المحوري والعينة المراد قياس ثابت العازل الكهربائي الخاص بها. قمنا باشتقاق تعبيراً رياضياً كاملاً للأشعة الكهرومغناطيسية المنتشرة داخل الموجِّه ومعامل الانعكاس من تقاطع الجزء المحوري بالموجِّه الدائري. استُخدِمَ في هذا العمل طريقة غالركن لايجاد التعبير الرياضي الخاص بمعامل الانعكاس من خلال الاستفادة من الشروط الحدية لتقاطع الموجِّه الدائري بالمحوري. ومن خلاله، ثابت العزل الكهربائي للعينة يتم ايجاده من المعكوس الرياضي لمعامل الانعكاس. لقد تم مقارنة الحل التحليلي المستنبط من هذه الرسالة مع الحل العددي المتوفر حاسوبياً و وجدنا توافقاً كبيراً. ايضاً تم اختبار الحل التحليلي لمعامل الانعكاس لعينة صخرية في المعمل و وجدنا تطابقاً بين الحل التحليلي وقياس المعمل عند تردد 1 ميجا هيرتز حتى 500 ميجا هيرتز.

CHAPTER 1

INTRODUCTION

In the oil field industry, *In-Situ* hydrocarbon saturation measurement is of high interest. It is used to quantify total oil in place. Dielectric measurement uses electromagnetic wave propagation into the reservoir formation and one technique to predict fluid saturation in reservoirs. One of the advantages of this technique is the ability to distinguish between water, (ε_r= 80), and oil (ε_r= 2).

There are two logging tools that use this principle: Electromagnetic Propagation Tool (EPT) and Array Dielectric Scanner Tool (ADT) both developed by Schlumberger [1, 2]. Several physical models have been developed to predict petrophyiscal information about the rock from Dielectric measurement such as: water-filled porosity, textural information, grain shape factor...etc. [3, 4, 5, 6]. These models either use single frequency measurement such as Complex Refractive index Model (CRIM) (Roth *et al.* [7]), or multi-frequency such as the model developed by *P. Sen* [8]. Therefore, a lot of effort in the last two decades has been made to obtain a rich database of dielectric measurement in the lab to develop more interpretation models for utilizing field data in addition to data validation purposes.

Most of the laboratory dielectric measurements on rocks were done on ambient conditions. Whereas rock's petrophysical properties such as grain shape factor or

wettability, which is a measure of fluids adhesion to rock surface, are dependent on pressure and temperature of fluids filling the rock. Hence, there is a significant demand to perform laboratory dielectric measurements at high pressure and temperature to represent exactly the reservoir conditions and hence improve multi-frequency dielectric physical modelling [9].

In this work, we will try to explore measurement techniques available in literature. The best measurement method will be selected which can measure wide-band frequency dependent dielectric constant while preserving rock's textural conditions and saturating fluids pressure and temperature. Then, we will address the issue of having gaps between the sample and confining structure and come up with a full-wave mathematical model that describes the electromagnetic fields inside the measurement structure under study. After we come up with explicit formulation for reflection coefficient (R_0) from the fields' formulation, we will compare our results with numerical Finite Element method (FEM) to benchmark our analytical solution. Furthermore, we will study the sensitivity of gap dimensions and dielectric properties on our model and try to compare it with the model which doesn't account for gap influence. Finally, we will try to establish some laboratory data and invert them to come up with dielectric constant from reflection coefficient data from real rock sample.

CHAPTER 2

LITERATURE REVIEW

Various laboratory measurement methods have been used to study the dielectric permittivity of materials. Some methods are destructive, for example crushing the sample into a powder or drilling a plug out of a core samples [10], and others are non-destructive, [11, 12]. There are resonant and non-resonant devices that can be used to measure the dielectric properties of the material at RF and microwave frequencies. The non-resonant devices operate at wider frequencies range and use some combination of reflection and transmission of RF power [10, 12, 13]. The operating range of frequencies of these devices is controlled by the size of the sample and whether the presence of higher order modes can be accounted for in the theoretical formulation. The majority of the available work in the literature is done using coaxial structures that can be modeled as TEM modes [13]. However, to perform measurement at the high pressure and high temperature reservoir conditions, closed waveguide and cavity structures have the advantage [11, 14].

2.1 Coaxial-Circular Waveguide Features and Limitations

Due to the porous nature of reservoir rocks, the dielectric properties are frequency and temperature dependent [1]. Hence, it's desirable to work on a dielectric measuring structure that features both pressure confinement and multi-frequency operation. Coaxial-Circular junction is one such structure that is described in Taherian R. *et al.* [11]. In this

configuration, fundamental TEM mode is excited from the coaxial part that impinges upon the junction between the coaxial and circular waveguide. Part of the RF energy transmits into the waveguide section and part is reflected back due to the impedance mismatch between the two parts of the structure. The impedance mismatch, and thus the reflection coefficient, depends on the magnetic permeability and dielectric permittivity of the sample (see Figure. 1). Measurement of the reflection coefficient along with a model is used to extract the constitutive properties of the sample. The model as developed in [11], assumes the sample completely fills up the waveguide which holds true for liquid samples. However, for solid samples, such as rock core plugs, there is an unavoidable gap that is usually filled with the same liquid as the one in the pore space of the rock. The model assumes the error caused by any such gap to be negligible. This requires the sample under test to be treated as one medium bound by the metallic waveguide. However in practice, this is hardly the case for solid samples. Therefore, the full-wave analysis developed in [16] should be modified to account for the proper boundary condition for the rock by accounting for the thin (liquid filled) layer surrounding the sample.

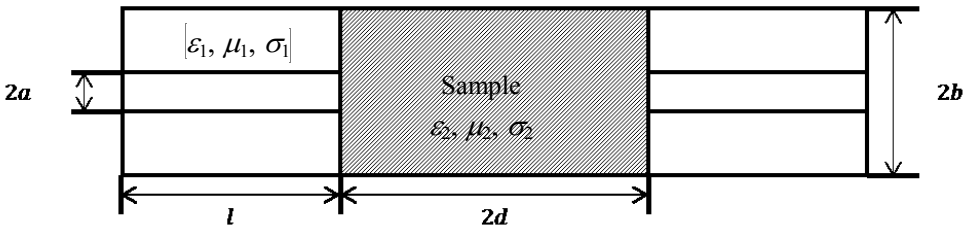

Figure 1 Schematic of the Coaxial-Circular Cell

2.2 Thin Layer Modelling in Dielectric Waveguides

Many authors studied the effect of the thin layer filling the circular waveguide longitudinally on EM fields' distribution. The case of cylindrically symmetric and centric two dielectrics filling an infinite metal tube has been studied by Pincherle [15] and Chambers [16] and for eccentric case can be found in H. Ragheb et al. work [17]. Also, similar analysis of gap effect has been published by Haung and Shen for sample loaded inside a coaxial line [18]. In this work, we follow a formulation similar to the one presented in Taherian R. *et al.* [11]. Only Reflection measurement is considered in our case and the thin layer is assumed to be cylindrically symmetric around the axis of the waveguide. Two cases will be considered: gap filled with lossless and lossy (conductive) material.

CHAPTER 3

THEORETICAL BACKGROUND

The configuration of the current problem is divided into two sections: A coaxial part and a circular waveguide filled longitudinally with two dielectrics terminated by a Perfect Electric Conductor (PEC), as shown in Figure 2. The z component of the electric and magnetic fields inside the two sections must satisfy the solution of the homogeneous scalar Helmholtz equation in cylindrical coordinate form (ρ, θ, z):

$$\frac{\partial^2\psi}{\partial\rho^2} + \frac{1}{\rho}\frac{\partial\psi}{\partial\rho} + \frac{1}{\rho^2}\frac{\partial^2\psi}{\partial\theta^2} + k^2\psi = 0 \tag{1}$$

where

$$k^2 = \omega^2\mu\varepsilon - k_z^2 \tag{2}$$

is the separation constant and ψ represents either E_z or H_z. The rest of constants are ω, μ, ε are the angular frequency, magnetic permeability and complex dielectric constant respectively. The phase constant in the guide is ($k_z = {}^{2\pi}/_{\lambda_z}$) and the variation $e^{-j(\omega t - k_z z)}$ is assumed for in all fields expressions with omitting time exponents heareafter for simplification purpose. Any solution of equation (1) can be written as a linear combination of the following function:

$$\psi = [A_m \cos m\theta + B_m \sin m\theta] Z_m(k\rho) e^{j(\omega t - k_z z)} \tag{3}$$

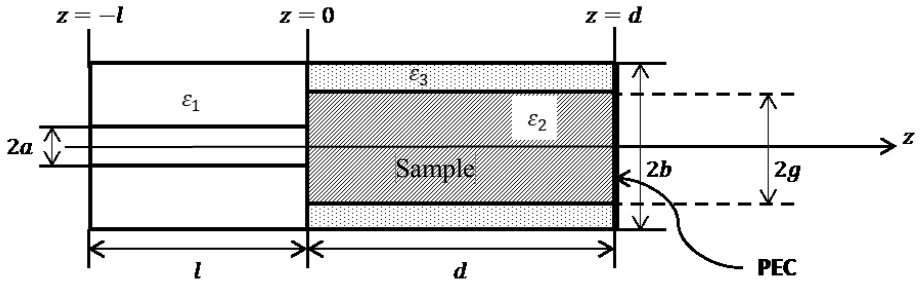

Figure 2 Configuration of coaxial to circular waveguide loaded longitudinally with two dielectrics

where $Z_m(k\rho)$ is the appropriate Bessel functions or a linear combination of them, and m is the harmonic order. Due to the azimuthal symmetry nature of the problem, the solution is independant of θ.

3.1 Coaxial Section Field Formulation

In Section 1 where we encounter a coaxial structure, we follow similar expression as in [11], where only incident and reflected TEM mode is assumed to propagate inside the coaxial line plus reflected TM modes resulting from the mode conversion at the boundary between the coaxial and the waveguide. The expression of the magnetic and electric fields in region 1 can be written as follows:

$$H_{1\theta} = \frac{1}{\eta_1} V_0\, \psi_{10}(\rho)\left[e^{jk_{1z}} - R_0 e^{-jk_{1z}}\right] - \omega\varepsilon_1 \sum_{n=1}^{\infty} \frac{1}{k_{1z_n}} A_n\, \psi_{1n}(\rho) e^{-jk_{1z_n}z} \tag{4a}$$

$$E_{1\rho} = V_0\, \psi_{10}(\rho)\left[e^{jk_{1z}} + R_0 e^{-jk_{1z}}\right] + \sum_{n=1}^{\infty} A_n\, \psi_{1n}(\rho) e^{-jk_{1z_n}z} \tag{4b}$$

$$E_{1z} = -j \sum_{n=1}^{\infty} \frac{k_{1\rho n}}{k_{1z_n}} A_n\, \psi_{0n}(\rho) e^{-jk_{1z_n}z} \tag{4c}$$

where $\psi_{0n}(\rho)$ and $\psi_{1n}(\rho)$ are the eignmode functions in the coaxial structure which are given as:

$$\psi_{0n}(\rho) = J_0(k_{1\rho_n}\rho)N_0(k_{1\rho_n}a) - J_0(k_{1\rho_n}a)N_0(k_{1\rho_n}\rho), \qquad n = 1, 2, 3, \ldots \quad (5a)$$

$$\psi_{1n}(\rho) = J_1(k_{1\rho_n}\rho)\, N_0(k_{1\rho_n}a) - J_0(k_{1\rho_n}a)\, N_1(k_{1\rho_n}\rho), \qquad n = 1, 2, 3, \ldots \quad (5b)$$

$$\psi_{10}(\rho) = \frac{1}{\rho} \quad (5c)$$

$k_{1\rho_n}$ is the solution of the eignmode function $\psi_{0n}(\rho)$ at $\rho = b$ in the coaxial section:

$$\psi_{0n}(b) = J_0(k_{1\rho_n}b)N_0(k_{1\rho_n}a) - J_0(k_{1\rho_n}a)N_0(k_{1\rho_n}b) = 0 \quad (6)$$

$k_{1\rho_n}$ and k_{1z_n} are related by the seperation equation:

$$[k_{1\rho_n}]^2 + [k_{1z_n}]^2 = k_1^2 = \omega^2\mu_0\varepsilon_1 \quad (7)$$

η_1 is the coaxial TEM impedance as defined by $\sqrt{\mu_0/\varepsilon_1}$ and ε_1 is the complex dielectric constant for the coaxial filling material.

3.2 Dielectric Loaded Circular Waveguide Section Field Formulation

The electric and magnetic fields representation in seection 2 and 3 are given as solutions of TM modes as presented in Pincherle L. formulation [15]. And only TM modes should be considered due to the excitation of the fields H_θ and E_ρ from the coaxial line. In representing the fields in section 2, we only have Bessel function of the first kind in the dielectric cyliner with the appropriate trigonometric function which vanishes the tangential electric fields at the PEC termination. The fields expressions can be written as:

$$H_{2\theta} = j\omega\varepsilon_2 \sum_{n=1}^{\infty} B_n J_1(k_{2\rho_n}\rho)\cos\{k_{2z_n}(d-z)\} \quad (8a)$$

$$E_{2\rho} = \sum_{n=1}^{\infty} B_n\, k_{2Z_n} J_1(k_{2\rho_n}\rho)\sin\{k_{2z_n}(d-z)\} \quad (8b)$$

$$E_{2z} = -\sum_{n=1}^{\infty} B_n \, k_{2\rho_n} \, J_0(k_{2\rho_n}\rho) \cos\{k_{2z_n}(d-z)\} \tag{8c}$$

For Section 3, we have to follow that E_θ and E_z must vanish at $\rho = b$ and so we can use a linear combination of Bessel and Neumann functions as follows:

$$H_{3\theta} = j\omega\varepsilon_3 \sum_{n=1}^{\infty} C_n \, \varphi_{1n}(\rho) \cos\{k_{2z_n}(d-z)\} \tag{9a}$$

$$E_{3\rho} = \sum_{n=1}^{\infty} C_n \, k_{2Z_n} \varphi_{1n}(\rho) \, \sin\{k_{2z_n}(d-z)\} \tag{9b}$$

$$E_{3z} = -\sum_{n=1}^{\infty} C_n \, k_{3\rho_n} \varphi_{0n}(\rho) \cos\{k_{2z_n}(d-z)\} \tag{9c}$$

where,

$$\varphi_{0n}(\rho) = J_0(k_{3\rho_n}\rho)N_0(k_{3\rho_n}b) - J_0(k_{3\rho_n}b)N_0(k_{3\rho_n}\rho) \tag{10a}$$

$$\varphi_{1n}(\rho) = J_1(k_{3\rho_n}\rho) \, N_0(k_{3\rho_n}b) - J_0(k_{3\rho_n}b) \, N_1(k_{3\rho_n}\rho) \tag{10b}$$

$$C_n = B_n \left(\frac{k_{2\rho_n}}{k_{3\rho_n}}\right) \frac{J_0(k_{2\rho_n}g)}{\varphi_{0n}(g)} = B_n \left(\frac{k_{2\rho_n}}{k_{3\rho_n}}\right) \frac{J_0(k_{2\rho_n}g)}{J_0(k_{3\rho_n}g) \, N_0(k_{3\rho_n}b) - J_0(k_{3\rho_n}b) N_0(k_{3\rho_n}g)} \tag{10c}$$

Hence,

$$H_{3\theta} = j\omega\varepsilon_3 \sum_{n=1}^{\infty} B_n \left(\frac{k_{2\rho_n}}{k_{3\rho_n}}\right) J_0(k_{2\rho_n}g) \frac{\varphi_{1n}(\rho)}{\varphi_{0n}(g)} \cos\{k_{2z_n}(d-z)\} \tag{11a}$$

$$E_{3\rho} = \sum_{n=1}^{\infty} B_n k_{2Z_n} \left(\frac{k_{2\rho_n}}{k_{3\rho_n}}\right) J_0(k_{2\rho_n}g) \frac{\varphi_{1n}(\rho)}{\varphi_{0n}(g)} \sin\{k_{2z_n}(d-z)\} \tag{11b}$$

$$E_{3z} = -\sum_{n=1}^{\infty} B_n k_{2\rho_n} J_0(k_{2\rho_n}g) \frac{\varphi_{0n}(\rho)}{\varphi_{0n}(g)} \cos\{k_{2z_n}(d-z)\} \tag{11c}$$

We can apply the boundary conditions at $\rho = g$ by enforcing the continuity of E_z and H_θ. In this case, we can get a relation between C_n and B_n as in (10c), also we can obtain the fundemantal equation for TM waves in the case of $m = 0$:

$$\frac{J_1(k_{2\rho_n} g)}{(k_{2\rho_n} g)\, J_0(k_{2\rho_n} g)} = \frac{\varepsilon_3}{\varepsilon_2 (k_{3\rho_n} g)} \frac{\varphi_{1n}(g)}{\varphi_{0n}(g)} \tag{12a}$$

$$\frac{J_1(k_{2\rho_n} g)}{(k_{2\rho_n} g)\, J_0(k_{2\rho_n} g)} = \frac{\varepsilon_3}{\varepsilon_2 (k_{3\rho_n} g)} \frac{J_0(k_{3\rho_n} b)\, N_1(k_{3\rho_n} g) - J_1(k_{3\rho_n} g)\, N_0(k_{3\rho_n} b)}{J_0(k_{3\rho_n} b)\, N_0(k_{3\rho_n} g) - J_0(k_{3\rho_n} g)\, N_0(k_{3\rho_n} b)} \tag{12b}$$

In equation (12) we can see that $k_{2\rho_n}$and $k_{2\rho_n}$ are related to each other. Also a seperation formula can be established in a similar manner as in (2) and (7) as follows:

$$[k_{3\rho_n}]^2 = [k_{2\rho_n}]^2 - \omega^2 \mu_0 (\varepsilon_2 - \varepsilon_3)\varepsilon_0 \tag{13}$$

From (12) and (13), we can determine the values of $k_{2\rho_n}$and $k_{3\rho_n}$and from equation (2) we can find k_{2z_n}.

From equation (12a) and equations (11), we get:

$$H_{3\theta} = j\omega\varepsilon_2 \sum_{n=1}^{\infty} B_n J_1(k_{2\rho_n} g)\, \frac{\varphi_{1n}(\rho)}{\varphi_{1n}(g)}\, \cos\{k_{2z_n}(d - z)\} \tag{14a}$$

$$E_{3\rho} = \frac{\varepsilon_2}{\epsilon_3} \sum_{n=1}^{\infty} B_n k_{2Z_n} J_1(k_{2\rho_n} g)\, \frac{\varphi_{1n}(\rho)}{\varphi_{1n}(g)}\, \sin\{k_{2z_n}(d - z)\} \tag{14b}$$

$$E_{3z} = -\sum_{n=1}^{\infty} B_n k_{2\rho_n} J_0(k_{2\rho_n} g) \frac{\varphi_{0n}(\rho)}{\varphi_{0n}(g)}\, \cos\{k_{2z_n}(d - z)\} \tag{14c}$$

We define the electromegnetic fields in the circular section $0 \le \rho \le b$ in terms of a composite basis function $\{\phi(\rho),\ 0 \le \rho \le b\}$ as follows:

$$H_{c\theta} = j\omega\varepsilon_2 \sum_{n=1}^{\infty} B_n \, \phi_{1n}(\rho) \cos\{k_{2z_n}(d-z)\} \tag{15a}$$

$$E_{c\rho} = \sum_{n=1}^{\infty} B_n \, k_{2z_n} \epsilon_r(\rho) \, \phi_{1n}(\rho) \sin\{k_{2z_n}(d-z)\} \tag{15b}$$

$$E_{cz} = -\sum_{n=1}^{\infty} B_n \, k_{2\rho_n} \phi_{0n}(\rho) \, \cos\{k_{2z_n}(d-z)\} \tag{15c}$$

where

$$\begin{aligned} \phi_{0n}(\rho) &= J_0(k_{2\rho_n}\rho), && 0 \le \rho \le g \\ &= \tfrac{\varphi_{0n}(\rho)}{\varphi_{0n}(g)} J_0(k_{2\rho_n} g), && g \le \rho \le b \end{aligned} \tag{16a}$$

$$\begin{aligned} \phi_{1n}(\rho) &= J_1(k_{2\rho_n}\rho), && 0 \le \rho \le g \\ &= \tfrac{\varphi_{1n}(\rho)}{\varphi_{1n}(g)} J_1(k_{2\rho_n} g), && g \le \rho \le b \end{aligned} \tag{16a}$$

$$\begin{aligned} \epsilon_r(\rho) &= 1, && 0 \le \rho \le g \\ &= \tfrac{\varepsilon_2}{\varepsilon_3}, && g \le \rho \le b \end{aligned} \tag{16c}$$

It is the composite basis function $\phi_n(\rho)$ that is orthogonal over $0 \le \rho \le b$.

Our goal now is to find a technique to compute the constants in each medium; A_n, B_n and the reflection coefficient R_0. We have a couple of techniques that we are going to discusss in the next section to compute those constants. With the knowledge of those constants, the fields inside the coaxial to circular waveguide junction with a gap surrounding the sample can be completely described.

CHAPTER 4

METHOD OF SOLUTION AND RESULTS

4.1 Boundary Value Problem

The solutions of the fields in structure under investigations as described in Figure 2 must satisfy the continuity at the boundaries. The boundary condition which we have to enforce is the coaxial line to dielectric waveguide junction, i.e. $z = 0$ as follows:

$$E_{c\rho}(\rho, z = 0) = 0, \qquad 0 \le \rho \le a$$
$$= E_{1\rho}(\rho, z = 0), \qquad a \le \rho \le b \tag{17a}$$

$$H_{1\theta}(\rho, z = 0) = H_{c\theta}(\rho, z = 0), \qquad a \le \rho \le b \tag{17b}$$

By substituting the fields expressions in (4), (8) and (14) into (17), we will have 3 sets of equations in 3 sets of unknowns, similar to the situation in [11]. With the aid of Galerkin's or any numerical method in which basis functions and orthogonality are utilized, one can write all expressions as functions of one variable with order n. Therefore we write a linear summation that can be expressed as a system of linear equation with degree n. Once the system is solved we can find the reflection coefficient R_0 from its relation with the solved constant.

Explicitly, equation (17a) is given by:

$$\sum_{n=1}^{\infty} B_n\, k_{2Z_n} \epsilon_r(\rho)\, \phi_{1n}(\rho)\, \sin\{k_{2z_n} d\} = 0, \qquad 0 \le \rho \le a$$

$$= E_{1\rho}(\rho, z = 0), \qquad a \le \rho \le b \quad (18)$$

This equation is different from the one in [11] due to the presence of the function $\epsilon_r(\rho)$ multiplying the basis function $\phi_{1n}(\rho)$. However, this equation can still be tested by the basis functions $\{\phi_{1n}(\rho)\}$ since they are complete (and orthogonal) over the cross-section of the circular waveguide section. In this case the left-hand side of equation (18) will be a full matrix when tested with $\{\phi_{1n}(\rho)\}$ rather than a diagonal matrix as in the previously referenced work [11].

First we test equation (17a) using the basis $\{\rho\phi_{1m}(\rho)\}$ to get:

$$\sum_{n=1}^{\infty} G_n\, M_{mn} = V_o(1 + R_o) Q_{m0} + \sum_{r=1}^{\infty} A_r\, Q_{mr} \quad (19)$$

Second we test equation (17b) using the basis $\{\rho\psi_{10}(\rho), \rho\psi_{1n}(\rho)\}$ to get:

$$\frac{1}{\eta_1} V_o(1 - R_o) N_0 = j\omega\varepsilon_2 \sum_{n=1}^{\infty} G_n\, f_n Q_{n0} \quad (20)$$

$$-\frac{\omega\varepsilon_1}{k_{1z_r}} A_r N_r = j\omega\varepsilon_2 \sum_{n=1}^{\infty} G_n\, f_n Q_{nr} \quad (21)$$

Where,

$G_n = k_{2zn} \sin(k_{2zn} d) B_n$

$f_n = \dfrac{1}{k_{2zn}} \cot(k_{2zn} d)$

$$M_{mn} = \int_a^b \rho\, \epsilon_r(\rho)\phi_{1m}(\rho)\phi_{1n}(\rho)d\rho$$

$$Q_{m0} = \int_a^b \rho\psi_{10}(\rho)\phi_{1m}(\rho)d\rho$$

$$Q_{mr} = \int_a^b \rho\psi_{1r}(\rho)\phi_{1m}(\rho)d\rho$$

$$N_0 = \int_a^b \rho[\,\psi_{10}(\rho)]^2 d\rho = \int_a^b \frac{1}{\rho}d\rho = \ln\left(\frac{b}{a}\right)$$

$$N_r = \int_a^b \rho[\,\psi_{1r}(\rho)]^2 d\rho = \frac{2}{(\pi k_{1\rho_r})^2}\left[\frac{J_0^2(k_{1\rho_n}a)}{J_0^2(k_{1\rho_n}b)} - 1\right], \qquad r \neq 0$$

The explicit solutions for the dot product integrals: M_{mn}, Q_{m0} and Q_{mr} are showed in Appendix 1. From (20) and (21), we can express A_r and R_0 as functions of G_n and then substitute the expressions in (19) to end up with a summation of linear equation in the form:

$$\sum_{n=1}^{\infty} U_{mn}D_n = 2Q_{m0} \tag{22}$$

Where,

$$D_n = j\frac{\varepsilon_2}{\varepsilon_1}\frac{1}{V_0}f_nG_n$$

$$U_{mn} = -j\frac{\varepsilon_1}{\varepsilon_2}g_nM_{mn} + \sum_{r=0}^{\infty} k_{1zr}\frac{Q_{mr}Q_{mr}}{N_r}$$

$$g_n = k_{2zn}\tan(k_{2zn}d)$$

$$k_{1z0} = k_1 = \omega\sqrt{\mu\varepsilon_1}$$

We can solve the matrix as in (22) using a computer program to get D_n. Also, we can get directly the reflection coefficient at the junction R_0 from:

$$R_0 = 1 - \frac{k_1}{N_0}\sum_{n=1}^{\infty} D_n Q_{n0} \tag{23}$$

If we want to compute R_0 in the measurement plane at the coaxial port, we can use the following formula as derived in [11].

$$S_{11} = R_0 e^{j2k_1 L} \tag{24}$$

Where L is the distance from coaxial-circular junction to the measurement port.

4.2 Forward Modelling

By developing a computer program using e.g. MATLAB, we can solve for the reflection coefficient at the measurement plane of the investigated structure, Figure 2, with known gap dimension and electrical properties. The MATLAB subroutines are listed in Appendix 2. Using mode truncating method, we can achieve an exact solution with a finite number of modes in the coaxial and dielectric loaded waveguide section. As an example, we solved for S_{11} using the proposed model of a case coaxial-circular structure with a coaxial filled with glass with dielectric constant (ε_1=5.1) and has a length of (L=23.88mm). The outer radius of the coaxial line is (b=19.055mm) and the inner conductor has a radius of (a=2.9mm) so that the coaxial characteristic impedance is 50Ohm [10]. The sample used for computing reflection coefficient has a dielectric constant of (ε_2=30), conductivity of (σ_2=0.5S/m) and length of (d=100mm) terminated

by a short (PEC). The gap is filled with lossless medium e.g. oil with dielectric constant (ε_3=2) and its thickness was varied to study the solution convergence for different gap dimensions.

In Figure 3, we can observe the solution convergence by fixing the number of waveguide modes, 50 modes, and vary coaxial modes at 1MHz operating frequency. The solutions converge faster for larger gap than smaller ones, though 40 coaxial modes are sufficient to show a converged solution for any gap dimension. Whereas at higher frequencies such as 500MHz, the convergence of the modes is not correlated to the gap thickness. Most probably due to the fact at higher frequency, the difference between ε_2 and ε_3 becomes negligible to change the propagation constant between the sample medium and the gap as from Equation (13). More sensitivity analysis will be carried in another section relating the gap and frequency effect to the solution.

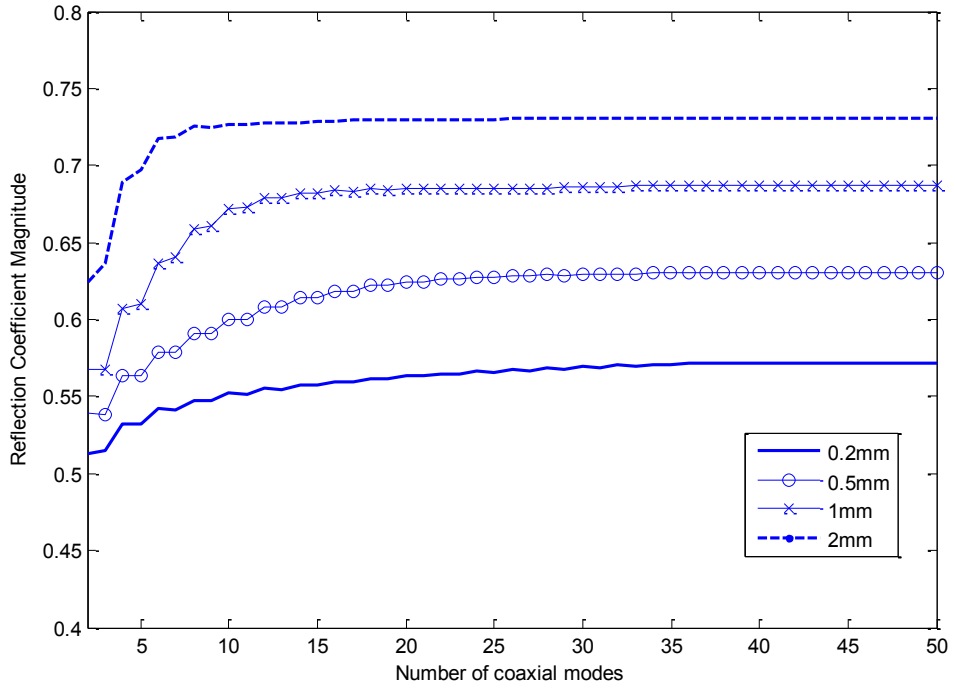

Figure 3 Solutions mode convergence at 1MHz for 50 waveguide modes for a gap with ε_r= 2 and different widths and sample under test of ε_r=30 and σ= 0.5S/m

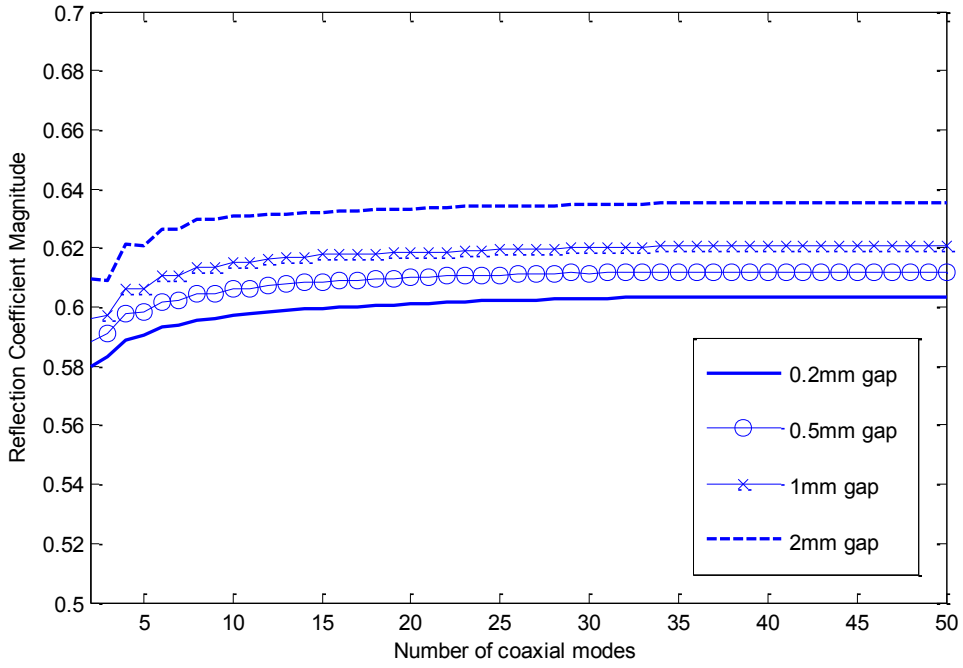

Figure 4 Solutions mode convergence at 500MHz for 50 waveguide modes for a gap with ε_r= 2 and different widths and sample under test of ε_r=30 and σ= 0.5S/m

4.3 Numerical Simulation and Results Verification

We have tested similar case as previously stated using RF module in COMSOL, a finite element ODE numerical solver. At first, we picked up the case of 1mm gap and frequency range of 1 to 1000 MHz. We compared the simulation reflection coefficient results with the one computed using the proposed model in this study in addition to the solution presented in previous work [11], see Figure 5, 6. When we compare between the solution of the model available in literature and COMSOL simulation, we see the 1mm gap can significantly change the measured reflection coefficient in most of our operating frequency band. Although at higher frequency, near 1GHz, the effect of gap reduces for S_{11} magnitude, still there is some noticeable variance in S_{11} value trend. However, when we take into account the gap effect as proposed in this study, we see good agreement between the simulation and our model on the entire frequency band with less than 2% tolerance for both amplitude and phase of the computed reflection coefficient.

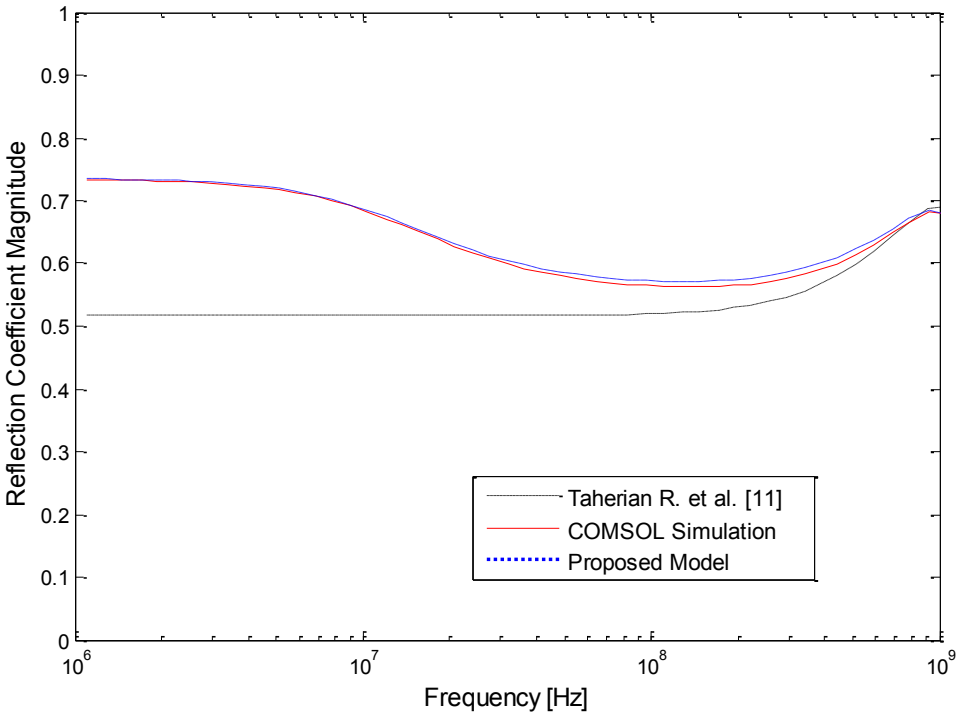

Figure 5 Comparison between the reflection coefficient magnitude from COMSOL simulation and computed using the proposed model which accounts for 1mm gap of ε_r= 2.

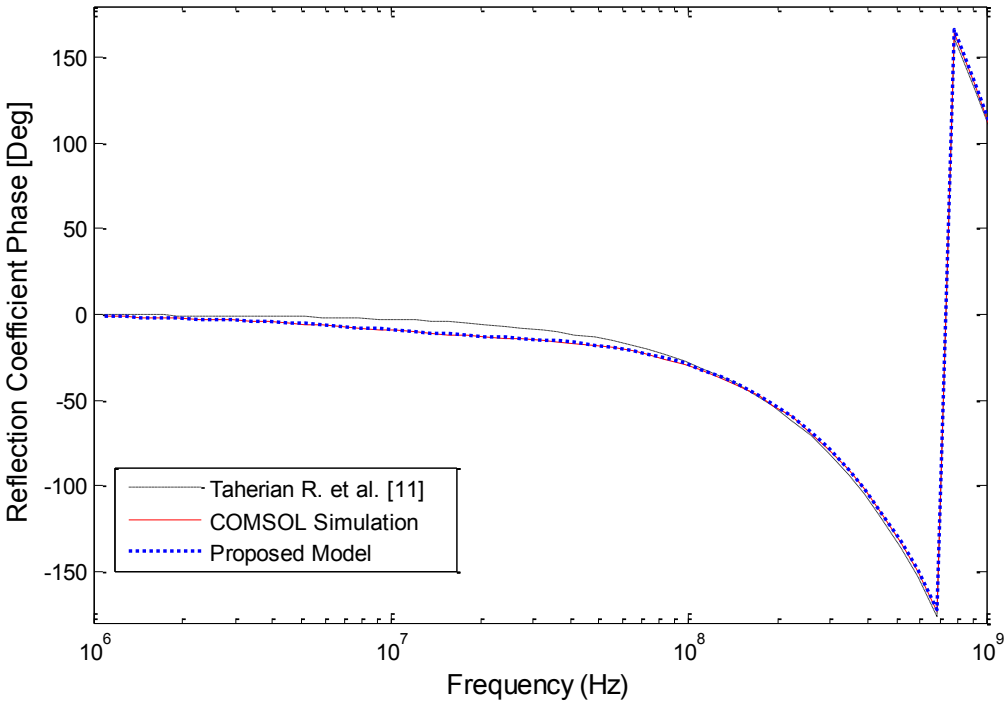

Figure 6 Comparison between the reflection coefficient phase from COMSOL simulation and computed using the proposed model which accounts for 1mm gap of ε_r= 2.

CHAPTER 5

RESULTS DISCUSSION AND ANALYSIS

5.1 Effect of Gap Thickness

The observed low frequency boost at low frequency was due to the finite thickness medium of lossless material which sets between the sample to be measured and the cylindrical waveguide wall. In this section, we assess the influence of the lossless gap dimension using similar sample and gap filling electrical properties and varying the gap thickness. Figure 7 shows the computed S_{11} using the proposed model compared to COMSOL simulation for different gap thicknesses in the frequency range 1 to 500MHz. Our results match very well the simulation outputs for whatever gap dimension. However, there is a range of frequencies where we can neglect the presence of the gap, this range depends highly on the gap thickness.

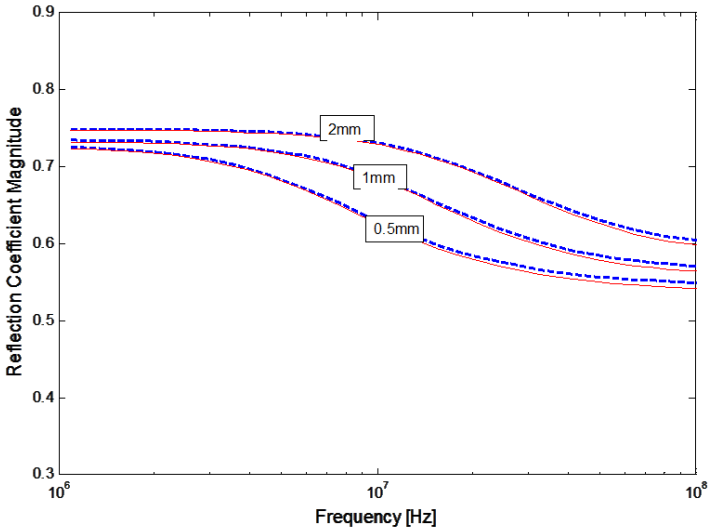

Figure 7 Comparison between simulation (solid line) and proposed model results (dashed line) for different gap thicknesses.

Generally, for a certain sample under test, the gap becomes negligible for very short wavelengths, i.e., when the waveguide acts as a dielectric waveguide. At that range of frequencies, we can approximate the solution of reflection coefficient to be close to the gapless configuration. In Figure 8, we plotted the wavelength of the waveguide for the mode E_{01}, which represents the fundamental mode, of the case of presence of different gaps, λ_g, versus the guide wavelength of gapless case, λ_0 ($\lambda_{0,g} = 2\pi/k_{2z_1}$). Both axes were normalized by the ratio ($\gamma = |\varepsilon_3/\varepsilon_2|$) to take the effect of dielectric constants of the two mediums out of the correlation. From the plot, we can observe λ_g for different gap dimensions starts to deviate from the gapless case λ_0 after certain critical point we call it critical wavelength, λ_c. The critical wavelength can be approximated from the correlation between λ_g and λ_0 for different gap dimensions at low frequency range. From Figure 9 we can see the low frequency trend can fit the power function:

$$y = ax^b \tag{25}$$

Exact values for a and b for each gap dimension are shown in Figure 9. To generalize this correlation for any gap dimension, we have to relate a and b with the gap thickness τ in mm. The value of b can be approximated to be constant and from Figure 9, we can see b ≈1.5 as a good approximate. Then, we fit the data again using Equation (25) with b=1.5 and correlate the result a from the fitting to gap thickness τ. The correlation between a and τ, see Figure 10, also follows power relation but with b=0.5, and can be written as:

$$a = 1.7439\sqrt{\tau} \tag{26}$$

Where τ is the gap thickness in mm. And the equation that relates wavelength at certain gap thickness to the gapless case wavelength in absolute values can be written as follows:

$$|\frac{\lambda_g}{\gamma}| = 1.7439\sqrt{\tau(|\frac{\lambda_0}{\gamma}|)^3} \tag{27}$$

To solve for the normalized critical wavelength (λ_c/γ), we use Equation (27) and substitute λ_0 by λ_g at which both are equal and hence we can approximate λ_c:

$$|\frac{\lambda_c}{\gamma}| = |\frac{1}{3.041\tau}| \tag{28}$$

So, we can approximate the wavelength in the waveguide of the coaxial-circular cell of dielectric material knowing its gap dimension and its wavelength for the completely filled waveguide as a piece-wise function as follows:

$$\lambda_g = 1.7439\sqrt{\tau(|\frac{\lambda_0}{\gamma}|)^3}, \qquad \lambda_g > \lambda_c$$

$$\lambda_g = \lambda_0\,, \qquad \lambda_g < \lambda_c \tag{29}$$

The approximation in (29) has an error which peaks around λ_c due to the transition from dielectric waveguide regime to hollow waveguide regime which is not characterized in this study. However, this error is fairly small as observed in Figure 11 which is below 1% based on the studied gap thicknesses, and around λ_c the error significantly increases up to 10%. Also, we can see $|\lambda_c/\gamma|$ for each corresponding gap thickness which increases as we reduce the gap as previously shown.

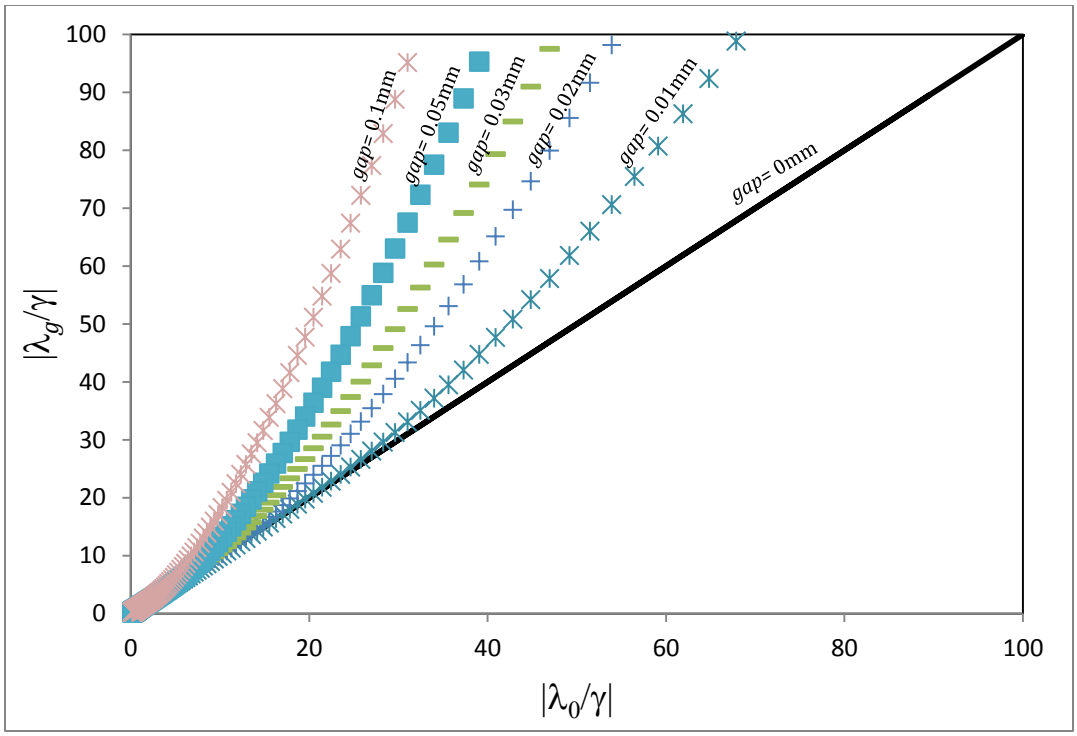

Figure 8 The relation between the wavelength in gapless medium and finite wall gap medium for different values of gap thickness, for the case of E_{01} TM mode.

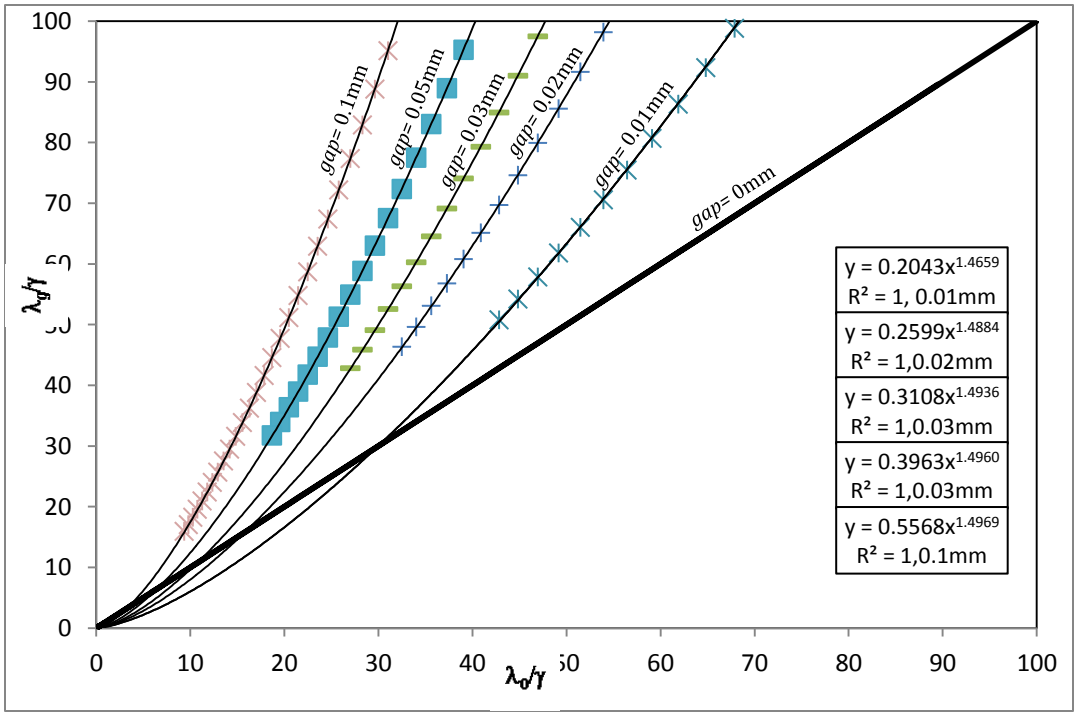

Figure 9 Low frequency data fitting for the relation between the wavelength of medium with different gap thickness and the gapless medium wavelength, data fitting by the power function (solid lines).

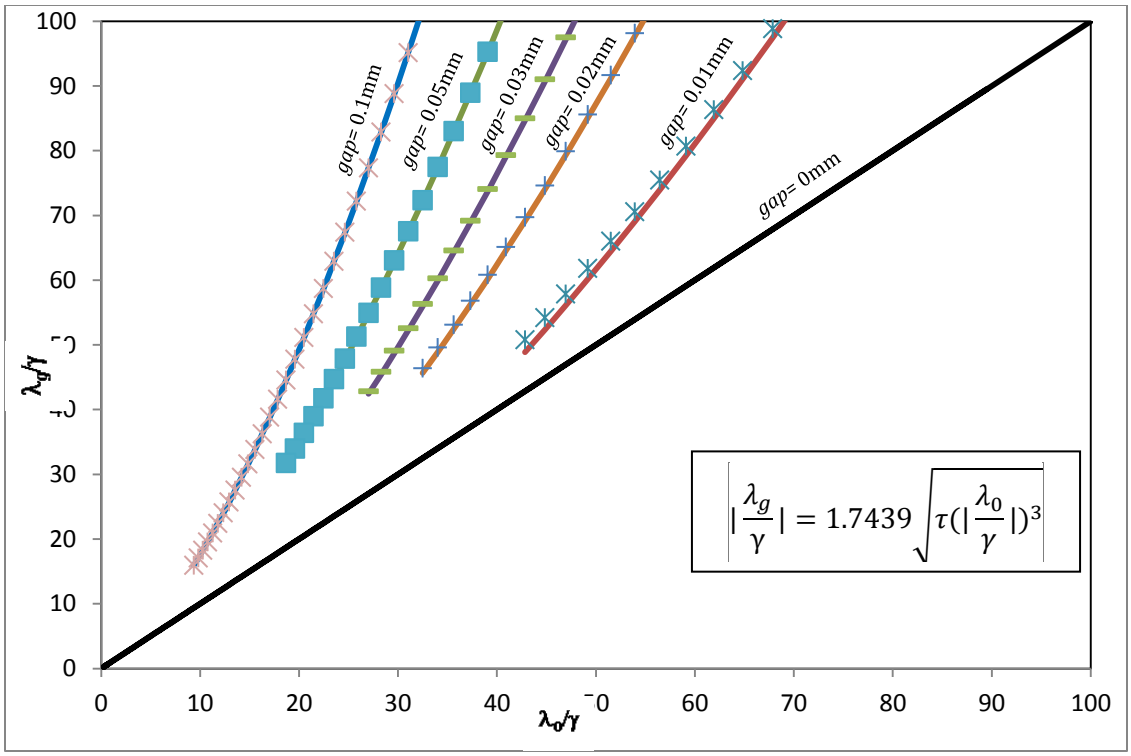

Figure 10 The proposed correlation to predict the wavelength of the guide for E_{01} mode in presence of a gap from the gapless guide wavelength, solid lines are the fitting of the approximation proposed.

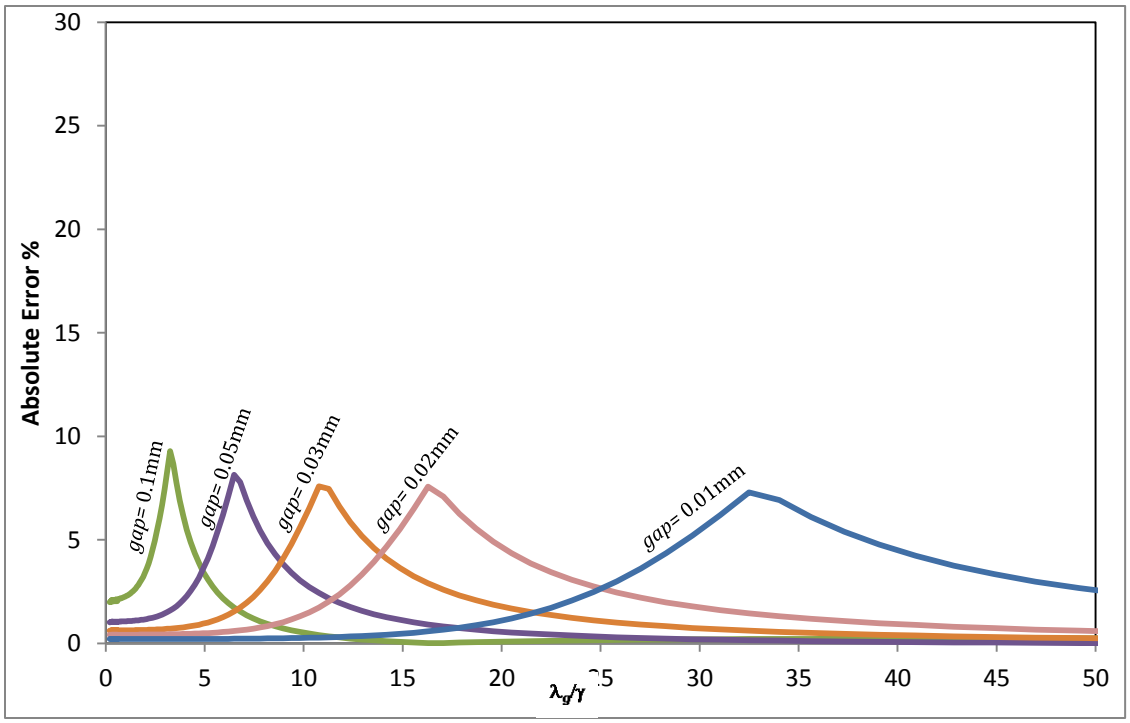

Figure 11 Error analysis of the proposed approximation on the normalized guide wavelength for different gap thickness.

5.2 Effect of Gap Dielectric Constant

The first case we treated was assumed that the gap is filled with a lossless gap such as oil. But when we fill the gap with a lossy or conductive medium which has higher complex permittivity magnitude than the sample under test, the wave propagation inside the sample will not be similar to the lossless gap due to the faster decay of EM fields in the conductive material.

For example, if we take the extreme case of the gap permittivity to be perfectly conductive, the waves propagate in the sample as if we shrink the waveguide diameter and reflect back as if it doesn't see the gap. The reflected fields from a PEC gap will be the same as no gap case if we assume the gap thickness is fairly small and higher modes scattering at the sharp edge of coaxial-circular interface is negligible. The Previous argument can be validated by assessing Equation (28). For a fixed gap dimension and the gap filled by PEC material, γ will be infinite and λ_c as well. So, the guide wavelength for the case of gap presence will be equal to the gapless case by referring to Equation (29).

When we fill the gap with relatively lower or higher dielectric constant medium, we can also use Equations (28) and (29) to approximate the guide wavelength. The critical wavelength will increase as the ratio γ increases. So if we want to blur or hide the gap effect and the experiment conditions allows, we can fill the gap with a lossy material such as brine water, which has a real dielectric constant with nominal value of 70 and conductivity dependent on its salinity and temperature and can vary between 0.1 and 20 S/m [5]. Figure 12 shows the magnitude and phase of the reflection coefficient of a sample with the same configuration as in section (4.2) but the lossless gap replaced with a

medium with dielectric constant of 70 and conductivity of 5 S/m. We can see the response is very close to the gapless case at the frequency range under study. Also we can use Equation (28) to compute the normalized critical wavelength $|\lambda_c/\gamma|$ for 1mm gap and was found to be 0.328. That is much higher than the actual normalized guide wavelength $|\lambda_g/\gamma|$ which is equal to 0.0498 at 1MHz. When we increase the frequency, $|\lambda_g/\gamma|$ will become even smaller. Thus, we can be sure that at the frequency range, 1MHz to 500MHz, the brine 1mm gap can be approximated to be invisible and that's clear from the agreement in Figure 12.

5.3 Sensitivity of Gap Dimension Uncertainty

In this section, we assess the residual error on the magnitude and phase of the reflection coefficient computed from the proposed model in this study in the case of gap dimension uncertainty. To do so, we assume we made an error of up to $\pm$5% in measuring the gap thickness and compare the result of reflection coefficient to that one coming from the actual dimension. We take the same case as presented in section (4.2) and vary the gap between 0.95mm to 1.05mm and evaluate the error related to the result of 1mm gap.

Figure 13 shows the error propagated to the magnitude and phase of the reflection coefficients. The 3D plots display the error as a function of thickness deviation and frequency. Our observation based on the computation of this example is that 5% error in gap size will translate to up to 1% error in magnitude and up to 5% error in phase. Generally, the error in gap measurement doesn't magnify in the reflection measurement data. Also, the error propagation decreases by factors at high frequency measurement

than the low frequency ones. That's probably at higher frequencies, the gap influence becomes smaller or insignificant.

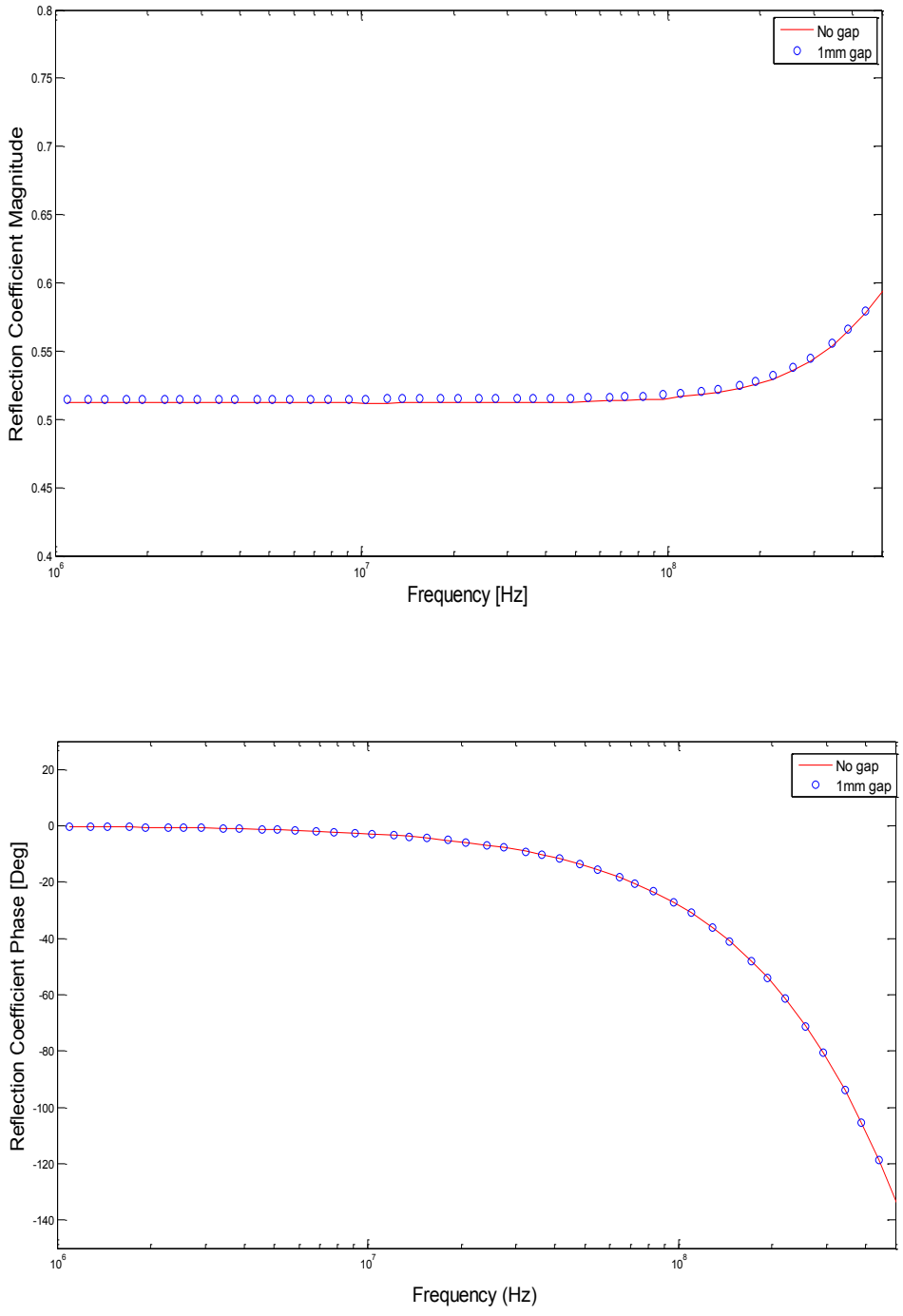

Figure 12 **Comparison between the reflection coefficient magnitude and phase of No gap solution and 1mm gap of brine ε_r= 70 and conductivity 5S/m.**

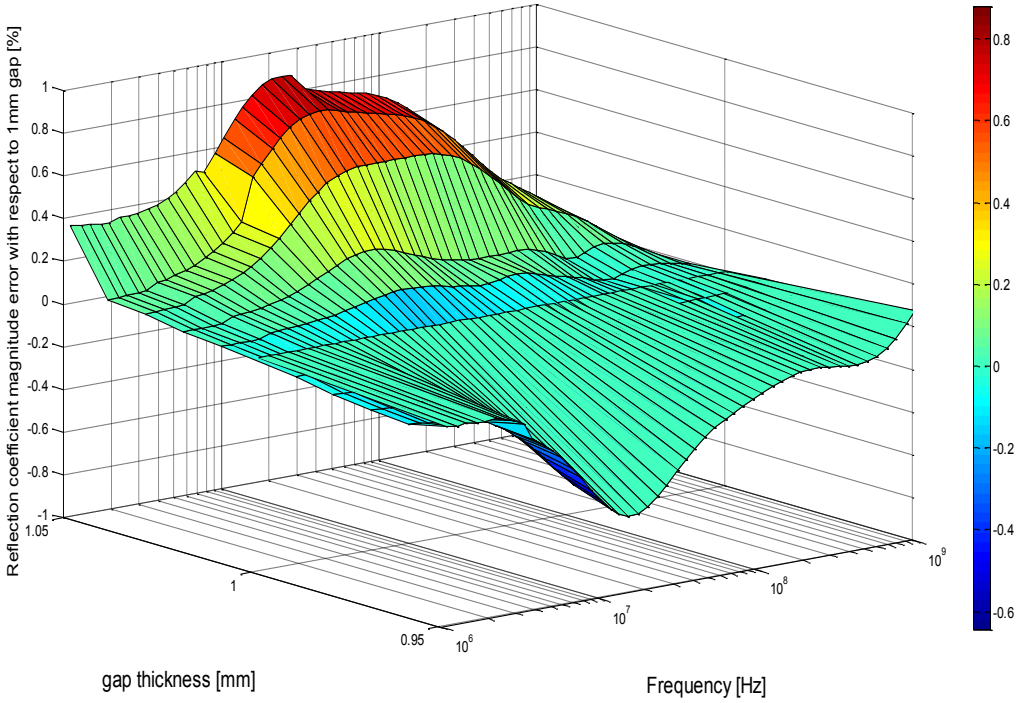

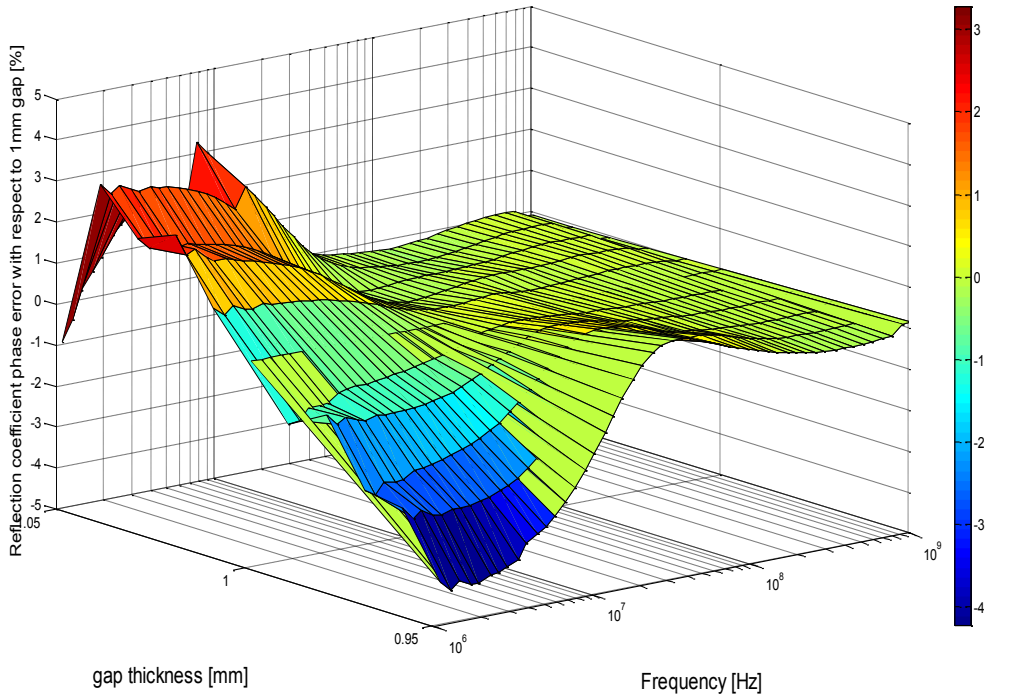

Figure 13 **Gap thickness uncertainty propagation to the magnitude and phase of reflection coefficient**

CHAPTER 6

EXPERIMENTAL MEASUREMENT AND DATA INVERSION

6.1 Experiment Apparatus

The experimental setup consists of two sections as shown in Figure 14. One section is the coaxial part whose outer conductor's diameter is 38mm and the inner conductor diameter is 6mm. Those dimensions have been designed to maintain 50ohm impedance to RF signals passing through the coaxial medium from the Vector Network Analyzer (VNA). The coaxial filling medium is fused glass that can hold high pressure and temperature conditions of the measurement. The other section of the system is a metallic core holder acts as a waveguide whose one end is open to the coaxial part and the other end is a metallic piston used to press on the sample. The diameter of the core holder is the same as the coaxial outer conductor. Detailed specifications of the experimental apparatus are shown in Table 1.

We can maintain the confining pressure on the sample by injecting fluid, distilled water typically, in the axial chamber which pushes the metallic piston toward the upper face of the sample making an axial stress. And due to having samples with diameter close to core holder's, the core holder will stop the sample from squeezing in the radial direction by reaction force of the thick metallic wall. The core holder is made of INCONEL and

15mm thick, its mechanical properties can hold radial stress more than 5000psi. For *in-situ* pore pressure, we have two valves on the side of the core holder which allow the passage of the pore fluids and one of them later can be closed to raise the pore pressure by injecting more fluid. The 24mm thick glass seal can hold the pressurized pore fluid from leaking to the RF measurement device. The system dimensions in previous analysis were chosen in accordance with the real system in the lab as described in Table 1.

Table 1 Experimental setup specifications

Setup Parameter	Value [units]
ε_1	5.1
ε_2	Sample to be measured
ε_3	2 (oil), 70(brine)
b	38.1 [mm]
a	5.8 [mm]
g	36.5 [mm]
d	50 [mm]
l	23.88 [mm]
s	13 [mm]

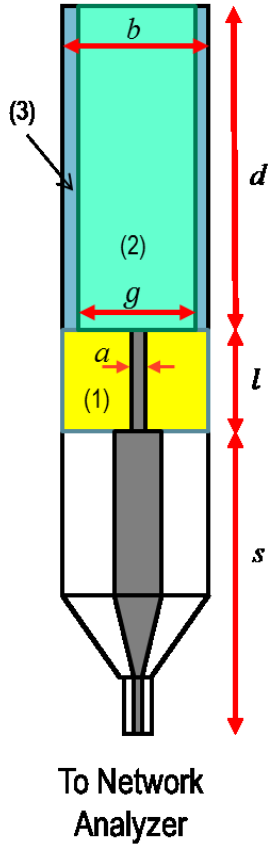

Figure 14 Schematic of laboratory HPHT coaxial-circular dielectric setup.

6.2 Experimental Procedure

During the experiment, the HPHT dielectric setup is positioned vertically so that RF section is at the bottom and injection of axial fluid is at the top. This position will make any air bubbles if exist escape up and away from the RF coaxial interface, also we can center the sample in the waveguide easily. Before start acquiring the measurement, we calibrate the VNA using three standard connectors: open, short and 50 Ohm load. After that, we begin loading the sample in the core holder and conduct the following steps to make the dielectric measurement at reservoir condition:

1. We place the core holder, including the fluid tubes, in an oven for the purpose of heating later.
2. Raise the axial pressure to a value that make sure the sample face is well coupled to the glass filled coaxial face at center position, here we used 100psi.
3. Inject 50psi or lower from the pore pressure valve inlet, we open the outlet couple of times to deplete the pressure and evacuate the cell from unnecessary gases.
4. Start to increase both axial and radial pressures gradually until we reach the required in situ pressure conditions. Here, we stopped at 3500psi axial pressure and 1500psi radial pressure.
5. We make dielectric measurement at ambient temperature.
6. Start heating the sample by setting the oven at the required temperature, 90 DegC in this study.
7. After the temperature of the sample stabilizes, we take the dielectric measurement at the high temperature.

We might repeat the measurement at high temperature if we suspect fluid distribution inside the sample still not stable or wait longer time until the fluids inside the rock settle down. For the sake of validating our model proposed here, we perform the measurement at ambient temperature once with oil pore pressure and another with water pore pressure.

That will give us two measurements, one with a lossy medium gap, i.e. brine (ε_r=70), and another with a lossless gap effect, i.e. oil (ε_r=2), which we are treating in this study. The S_{11} measurement for the two experiments is shown in Figure 15. We can see a significant discrepancy between the two measurements for the magnitude, but the phase is hardly influenced. That finding proves that there is a significant bias to the measurement due to the lossless gap, while the measurement with lossey gap is considered to be more representing the property of the rock without any bias following the discussion in Ch. 5.

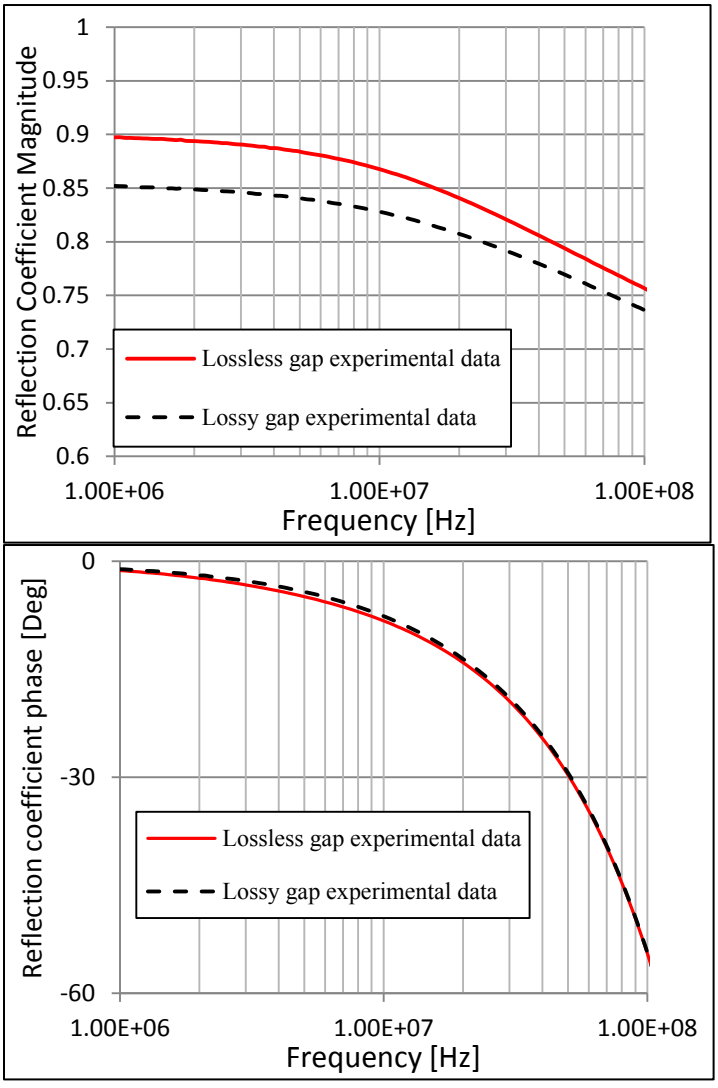

Figure 15 Experimental S_{11} measurements on rock sample at fixed condition but different gap fluid filling

6.3 Lab Measurement Validation and Data Inversion

In order to validate the reflection coefficient lab measurement from the described cell, we have to invert the reflection amplitude and phase data with a lossy gap experiment first. We can follow the inversion procedure described in [11, 13] using Newton-Raphson method or Levenberg-Marquardt available in MATLAB package with the proposed forward model in this study. The output of this inversion is the complex dielectric constant $\varepsilon^*(f)$ representing the homogeneous medium inside the circular waveguide and the solution of the following nonlinear expression:

$$F\big(\varepsilon^*(f)\big) = R_0\big(\varepsilon^*(f)\big) - R_{0(m)}(f) = 0 \tag{30}$$

where $R_{0(m)}$ is the measured reflection coefficient and R_0 is the forward problem solution of the reflection coefficient described in Equation (23) for a specific medium with permittivity ε^* surrounded by a known gap. As we approved in the previous chapter, section (5.2), that sample measurement with a lossy gap is very close to the actual sample measurement without a gap, we can use the inverted dielectric constant as our true and reference value representing the rock sample. Now, we can reproduce the reflection coefficient (S_{11}) for the 0.8mm oil gap measurement. In Figure 16, the forward model results show good agreement with lab measurement data. Small discrepancy between our forward model and the lab measurement can be due to changing fluid saturations while substituting the gap filling fluid from brine to oil.

Another way to validate the proposed forward model against the experimental data is to invert the measurement with lossless gap one time with gap attributes entered into the

model and another with discarding the gap presence. The two inverted permittivity and conductivity are compared against the lossy gap inversion. By this mean, we can see the effect of the lossless gap on the inverted dielectric properties of the sample. Also, we can assess the efficiency of our forward model to reproduce accurate dielectric constant from lab measurement exhibiting lossless wall gap. From Figure 17, the inverted real permittivity and conductivity from lossless gap data using the proposed forward model shows good agreement with the sample measurement with lossy gap. The discrepancy in the results at low frequency permittivity can be due to attributed to significant Signal-to-Noise ratio (SNR) of the measurement because the wavelength becomes larger than the sample length. On other hand, the inverted data with discarding the lossless gap effect show visible disagreement with error about 30% in conductivity at 2MHz and 20% of permittivity error at the same frequency. At higher frequencies, the errors reduce due to gap effect reduction as discussed earlier.

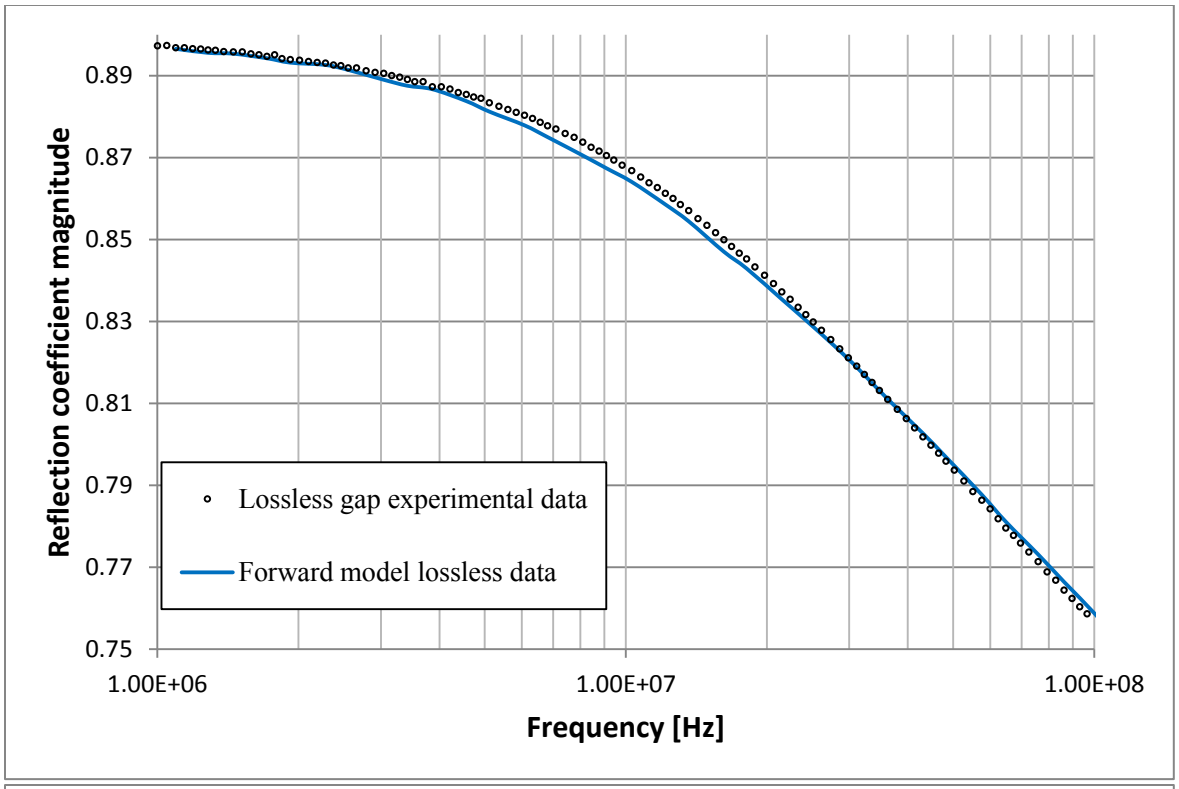

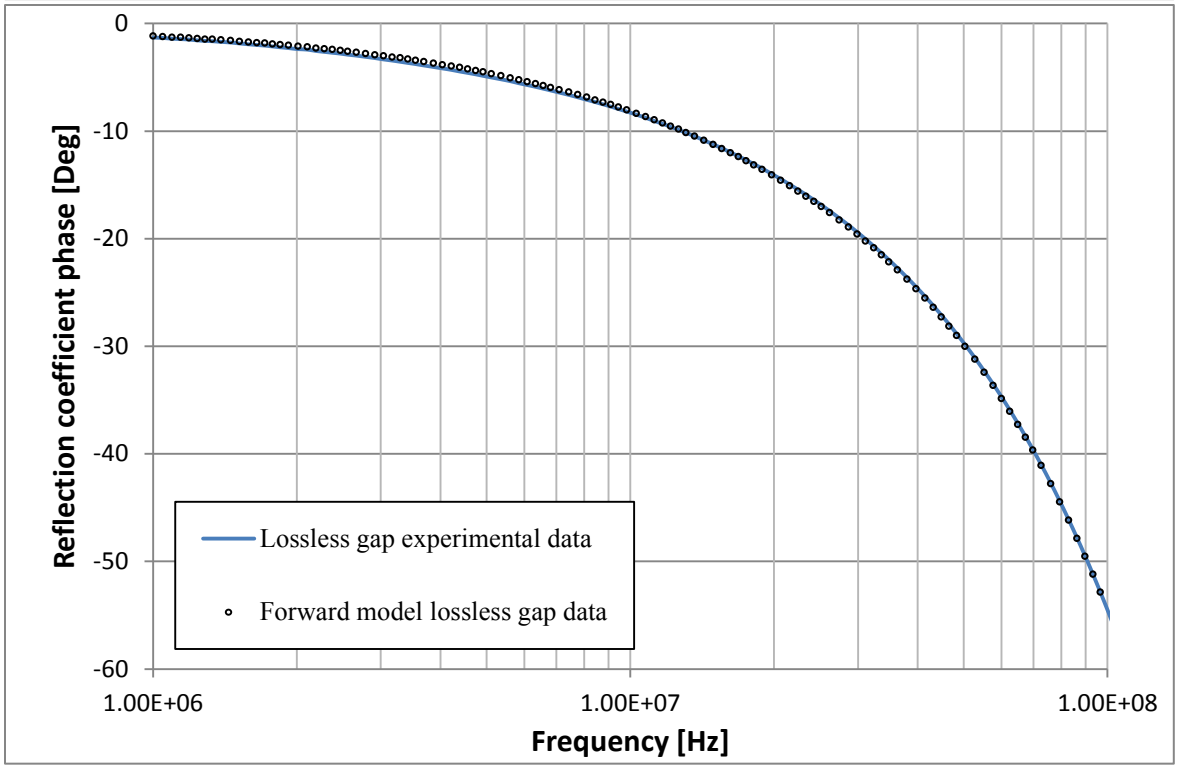

Figure 16 **Comparison between experimental results of limestone sample surrounded by 0.8mm oil gap and forward model prediction for S_{11} magnitude and phase. The measurement is done up to 500MHz but since the experimental and numerical data are collapsing after 100MHz, it has been excluded.**

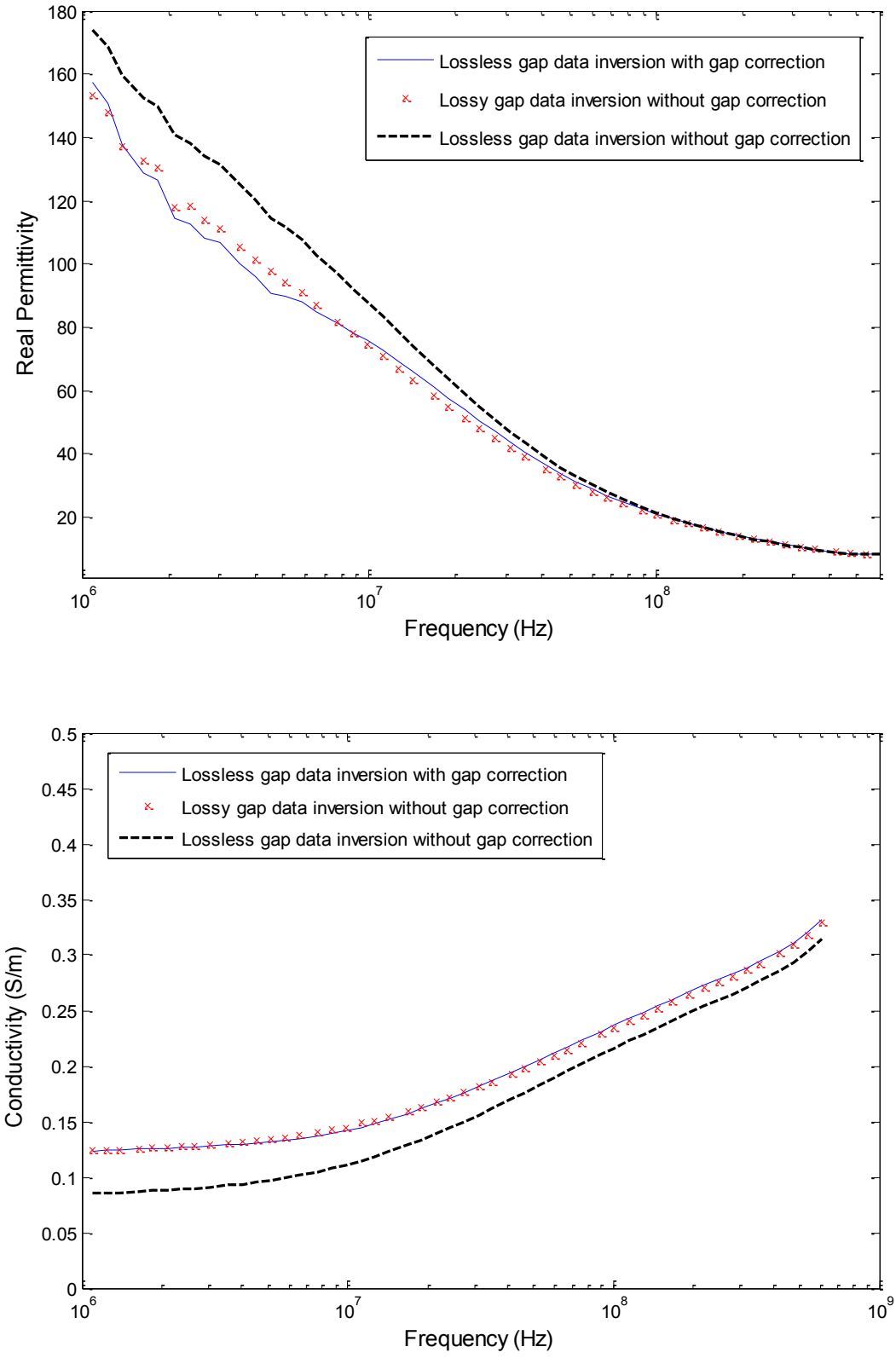

Figure 17 **Real permittivity and conductivity inversion from lossless gap and lossy gap data.**

CHAPTER 7

CONCLUSIONS

7.1 Final Remarks

In this work we analyzed the effect of dielectric gap separating a sample under test in a coaxial to circular waveguide cell. The expression of reflection coefficient was formulated after the introduction of centric and symmetric medium around the sample with known thickness. The forward solution from the proposed model was benchmarked with numerical simulation from COMSOL. We evaluated the solution convergence against the number of modes considered in the model and we found out 40 coaxial TM modes and 50 circular waveguide TM modes is adequate for whatever gap thickness. Also, we studied the effect of gap dimension and dielectric properties on the measurement and we come up with approximating formula to predict the effect of the gap with known thickness on the measurement of homogeneous coaxial to circular waveguide model. Furthermore, we examined the error propagation of gap dimension uncertainty on the measured reflection coefficient and we found the error propagates lower at higher frequency as we reduce the influence of the gap on the measurement. The cut-off frequency when we start seeing an effect of the gap is evaluated and found to be a function of the ratio of the sample and gap dielectric constants, and gap thickness. Furthermore, we established some experimental measurement at high pressure condition for a sample with a wall gap from coaxial to circular waveguide cell. The inverted

dielectric constant and conductivity dispersions from measurement based on a lossless gap agrees very well with the results from a lossy gap which is not influenced by the gap.

7.2 Way Ahead Recommendations

There are a lot of potential to use the developed analytical model to solve for dielectric contestant dispersion under reservoir conditions in the lab. The model has some limitation by assuming the sample to be symmetric and centric. Solving for off-centered sample loading into the waveguide will be very helpful to account for centering uncertainty. This problem might be very involved mathematically due to the lack of symmetry in azimuthal direction. Also, we have shown that we can invert for complex dielectric constant from laboratory data and even if our model which accounts for gap presence give better result than the model which doesn't, we still need to quantify the tolerance and errors that can influence our inverted results. Furthermore, our setup was analyzed in reflection mode, one can solve the gap effect on transmission mode measurement in case the sample is coupled by coaxial line from the two ends. This work also can be continued and used for better petrophysical modelling of reservoir rocks since we can measure the rock samples under reservoir conditions more reliably.

References

[1] Mehdi, H. et al. “Dielectric Dispersion: A New Wireline Petrophysical Measurement”, paper SPE 116130 Denver, Colorado, USA, 21–24 September 2008.

[2] Wharton, R.P. et al., "Electromagnetic Propagation Logging: Advances in Technique and Interpretation" paper SPE 9267 presented at the 1980 SPE Annual Technical Conference and Exhibition, Dallas, Sept. 21-24.

[3] Kenyon, W.E., “Texture effects on megahertz dielectric properties of calcite rock samples”, J. Appl. Phys 1984, 55(8) 3153-3159.Kenyon, W.E., “Texture effects on megahertz dielectric properties of calcite rock samples”, J. Appl. Phys 1984, 55(8) 3153-3159.

[4] Seleznev, N. et al., “Formation properties derived from multi-frequency dielectric measurement”. Paper VVV. SPWLA Annual Logging Symposium, Veracruz, Mexico 4-7 June 2006.

[5] Seleznev ,N., “Dielectric mixing laws for fully and partially saturated carbonates rocks “ SPWLA 45th Annual Logging Symposium, 2004.

[6] Shechao Feng and P.N. Sen, “Geometrical model of conductivity and dielectric properties of partially saturated rocks”, J. Appl. Phys. 58 (8) 15 October 1985 p3236.

[7] Roth, K., R. Schulin, H. Fluhler, and W. Attinger, “Calibration of time domain reflectometry for water content measurement using a composite dielectric approach”, Water Resour. Res., 26, 2267– 2273, 1990.

[8] Sen P.N., “Relation of Certain Geometrical Features to the dielectric anomaly of rocks”, Geophysics 1981, 46(12) 1714-1720.

[9] Schmitt, D.P., et al., “Revisiting dielectric logging in Saudi Arabia: recent experiences and applications in development and application wells”. Presented at the SPE/DGS Saudi Arabia Section Technical Symposium and Exhibition, SPE 149131, May 2011.

[10] Shen L. C., “A laboratory technique for measuring dielectric properties of core samples at ultra-high frequencies”, SPE 12552, 1983.

[11] Taherian R., Habashy, T., Yuen J., Kong J., “A coaxial-circular waveguide for dielectric measurement”, IEEE Trans. Geoscience and Remote Sensing, vol.29, No.2, 321-330, 1991.

[12] Stuchly, M. A. and Stuchly, S. S., “Coaxial line reflection methods for measuring dielectric properties of biological substrates at radio and microwave frequencies-a review”, IEEE Trans. Instrum. Meas., vol. IM-29, pp. 176-183, June 1980.

[13] Belhadj-Tahar, N. E., Foumer-Lamer A., and Chanterac H., “Broad-band simultaneous measurement of complex permittivity and permeability using a coaxial discontinuity”, IEEE Trans. Microwave Theory Tech., vol. 38, pp. 1-7, Jan. 1990.

[14] Works, C.N., Dakin, T.W., and Boggs, F.W.: "A Resonant-Cavity Method for Measuring Dielectric Properties at Ultra High Frequencies", Proc., I.R.E. (April 1945), 245-54; Trans., A.I.E.E., 63, 1092-98.

[15] PINCHERLE, L., “Electromagnetic waves in metal tubes filled longitudinally with two dielectrics”, Phys. Rev., 1944, 66, pp. 118-130.

[16] CHAMBERS, LL. G., “Propagation in waveguides filled longitudinally with two or more dielectrics”, Brit. J. Appl. Phys., 1953, 4, nn. 39-45.

[17] Ragheb H.A., Sebak A., Shafai L., “Cutoff frequencies of circular waveguide loaded with eccentric dielectric cylinder”, IEE Proc-Microw. Antennas Propagation., Vol. 144, No. 1 Feb. 1997.

[18] Huang, F.S.C. and Shen, L.D., "Analysis of Error Due to Presence of Gaps in the Measurement of Rock Samples in a Coaxial Line," Geophysics, 1983, 48, No.2, 206-12.

Vitae

Name	: Salah Mohammed Al-Ofi
Nationality	: Saudi
Date of Birth	:11/19/1987
Email	: sal-ofi@slb.com
Address	: P.O. Box 39011, Dammam / Doha Camp 31942

Academic Background : I obtained BSc degree in Electrical Engineering in 2009 from KFUPM with first honor. Then I join Schlumberger in R&D department in 2010 as a Research Associate working on subsurface characterization research. With this position, I co-authored two journal papers, one patent application and two conference papers. My research is related to solving electromagnetic problems in heterogeneous subsurface medium and developing lab measurements for electrical and mechanical properties prediction of sediment rocks. I'm an active member of IEEE and Society of Petroleum Engineers (SPE).

Appendix 1

Mathematical Formulation of some Dot Product Integrals of Bessel Functions

1. $M_{mn} = \int_a^b \rho\, \epsilon_r(\rho)\phi_{1m}(\rho)\phi_{1n}(\rho)d\rho$:

for $\boldsymbol{m = n}$

$$M_{mn} = \int_0^g \rho\, J_1^2(k_{2\rho m}\rho)d\rho + \frac{\varepsilon_2}{\varepsilon_3}\left(\frac{J_1(k_{2\rho m}g)}{\varphi_{1m(g)}}\right)^2 \int_g^b \rho\, [J_1(k_{3\rho m}\rho)N_0(k_{3\rho m}b) - J_0(k_{3\rho m}b)N_1(k_{3\rho m}\rho)]^2 d\rho$$

$$= \frac{1}{2}\left[g^2 J_0^2(k_{2\rho m}g) + g^2 J_1^2(k_{2\rho m}g) - \frac{2g}{k_{2\rho m}} J_0\,(k_{2\rho m}g) J_1\,(k_{2\rho m}g)\right] + \frac{\varepsilon_2}{\varepsilon_3}\left(\frac{J_1(k_{2\rho m}g)}{\varphi_{1m(g)}}\right)^2 (A - 2B + C)$$

$$A = \frac{N_0^2(k_{3\rho m}b)}{2}[\rho^2 J_0^2(k_{3\rho m}\rho) + \rho^2 J_1^2(k_{3\rho m}\rho) - \frac{2\rho}{k_{3\rho m}} J_0(k_{3\rho m}\rho)J_1(k_{3\rho m}\rho)]_g^b$$

$$B = \frac{N_0(k_{3\rho m}b)J_0(k_{3\rho m}b)}{2}[\rho^2 N_0(k_{3\rho m}\rho)J_0(k_{3\rho m}\rho) + \rho^2 N_1(k_{3\rho m}\rho)J_1(k_{3\rho m}\rho) - \frac{2\rho}{k_{3\rho m}} N_1(k_{3\rho m}\rho)J_0(k_{3\rho m}\rho)]_g^b$$

$$C = \frac{J_0^2(k_{3\rho m}b)}{2}[\rho^2 N_0^2(k_{3\rho m}\rho) + \rho^2 N_1^2(k_{3\rho m}\rho) - \frac{2\rho}{k_{3\rho m}} N_0(k_{3\rho m}\rho)N_1(k_{3\rho m}\rho)]_g^b$$

for $m \neq n$

$$M_{mn} = \int_0^g \rho J_1(k_{2\rho m}\rho) J_1(k_{2\rho n}\rho) d\rho$$

$$+ \frac{\varepsilon_2}{\varepsilon_3}\left(\frac{J_1(k_{2\rho m}g)J_1(k_{2\rho n}g)}{\varphi_{1m(g)}\varphi_{1n(g)}}\right)\int_g^b \rho\,[J_1(k_{3\rho m}\rho)N_0(k_{3\rho m}b)$$

$$- J_0(k_{3\rho m}b)N_1(k_{3\rho m}\rho)].[J_1(k_{3\rho n}\rho)N_0(k_{3\rho n}b) - J_0(k_{3\rho n}b)N_1(k_{3\rho n}\rho)]d\rho$$

$$= \frac{g}{\{k_{2\rho m}\}^2 - \{k_{2\rho n}\}^2}[k_{2\rho n}J_1(k_{2\rho m}g)J_0(k_{2\rho n}g) - k_{2\rho m}J_0(k_{2\rho m}g)J_1(k_{2\rho n}g)]$$

$$+ \frac{\varepsilon_2}{\varepsilon_3}\left(\frac{J_1(k_{2\rho m}g)J_1(k_{2\rho n}g)}{\varphi_{1m(g)}\varphi_{1n(g)}}\right)(D - E - F + G)$$

$$D = \frac{N_0(k_{3\rho m}b)N_0(k_{3\rho n}b)}{\{k_{3\rho m}\}^2 - \{k_{3\rho n}\}^2}[\rho k_{3\rho n}J_1(k_{3\rho m}\rho)J_0(k_{3\rho n}\rho) - \rho k_{3\rho m}J_0(k_{3\rho m}\rho)J_1(k_{3\rho n}\rho)]_g^b$$

$$E = \frac{J_0(k_{3\rho m}b)N_0(k_{3\rho n}b)}{\{k_{3\rho n}\}^2 - \{k_{3\rho m}\}^2}[\rho k_{3\rho m}J_1(k_{3\rho n}\rho)N_0(k_{3\rho m}\rho) - \rho k_{3\rho n}J_0(k_{3\rho n}\rho)N_1(k_{3\rho m}\rho)]_g^b$$

$$F = \frac{N_0(k_{3\rho m}b)J_0(k_{3\rho n}b)}{\{k_{3\rho m}\}^2 - \{k_{3\rho n}\}^2}[\rho k_{3\rho n}J_1(k_{3\rho m}\rho)N_0(k_{3\rho n}\rho) - \rho k_{3\rho m}J_0(k_{3\rho m}\rho)N_1(k_{3\rho n}\rho)]_g^b$$

$$G = \frac{J_0(k_{3\rho m}b)J_0(k_{3\rho n}b)}{\{k_{3\rho m}\}^2 - \{k_{3\rho n}\}^2}[\rho k_{3\rho n}N_1(k_{3\rho m}\rho)N_0(k_{3\rho n}\rho) - \rho k_{3\rho m}N_0(k_{3\rho m}\rho)N_1(k_{3\rho n}\rho)]_g^b$$

2. $Q_{m0} = \int_a^b \rho\psi_{10}(\rho)\phi_{1m}(\rho)d\rho$:

$$Q_{m0} = \int_a^g \rho\psi_{10}(\rho)\phi_{1m}(\rho)d\rho + \int_g^b \rho\psi_{10}(\rho)\phi_{1m}(\rho)d\rho = H_1 + H_2$$

$$H_1 = \int_a^g J_1(k_{2\rho m}\rho)d\rho = \frac{1}{(k_{2\rho m})}[J_0(k_{2\rho m}a) - J_0(k_{2\rho m}b)]$$

$$H_2 = \int_g^b \frac{J_1(k_{2\rho m}g)}{\varphi_{1m}(g)}\varphi_{1m}(\rho)d\rho = \left[\frac{J_1(k_{2\rho m}g)}{\varphi_{1m}(g)}\right]\int_g^b [N_0(k_{3\rho m}b)J_1(k_{3\rho n}\rho) - J_0(k_{3\rho m}b)N_1(k_{3\rho m}\rho)]d\rho$$

$$= \frac{J_1(k_{2\rho m}g)\varphi_{0m}(g)}{k_{3\rho m}\varphi_{1m}(g)}$$

3. $Q_{mr} = \int_a^b \rho\psi_{1r}(\rho)\phi_{1m}(\rho)d\rho$:

$$Q_{mr} = \int_a^g \rho\psi_{1r}(\rho)\phi_{1m}(\rho)d\rho + \int_g^b \rho\psi_{1r}(\rho)\phi_{1m}(\rho)d\rho = K_1 + K_2$$

$$K_1 = N_0(k_{1\rho r}a)\int_a^g \rho J_1(k_{1\rho r}\rho)J_1(k_{2\rho m}\rho)d\rho - J_0(k_{1\rho r}a)\int_a^g \rho N_1(k_{1\rho r}\rho)J_1(k_{2\rho m}\rho)d\rho = AK_1 - BK_1$$

$$AK_1 = \frac{N_0(k_{1\rho r}a)}{\{k_{1\rho r}\}^2 - \{k_{2\rho m}\}^2}[\rho k_{2\rho m}J_1(k_{1\rho r}\rho)J_0(k_{2\rho m}\rho) - \rho k_{1\rho r}J_0(k_{1\rho r}\rho)J_1(k_{2\rho m}\rho)]_a^g$$

$$BK_1 = \frac{J_0(k_{1\rho r}a)}{\{k_{2\rho m}\}^2 - \{k_{1\rho r}\}^2}[\rho k_{1\rho r}J_1(k_{2\rho m}\rho)N_0(k_{1\rho r}\rho) - \rho k_{2\rho m}J_0(k_{2\rho m}\rho)N_1(k_{1\rho r}\rho)]_a^g$$

$$K_2 = \left[\frac{J_1(k_{2\rho m}g)}{\varphi_{1m}(g)}\right]\int_g^b \rho\left[J_1(k_{1\rho r}\rho)N_0(k_{1\rho r}a) - J_0(k_{1\rho r}a)N_1(k_{1\rho r}\rho)\right]\left[N_0(k_{3\rho m}b)J_1(k_{3\rho n}\rho)\right.$$

$$\left. - J_0(k_{3\rho m}b)N_1(k_{3\rho m}\rho)\right]d\rho = \left[\frac{J_1(k_{2\rho m}g)}{\varphi_{1m}(g)}\right][AK_2 - BK_2 - CK_2 + DK_2]$$

$$AK_2 = \frac{N_0(k_{1\rho r}a)N_0(k_{3\rho m}b)}{\{k_{1\rho r}\}^2 - \{k_{3\rho m}\}^2}[\rho k_{3\rho m}J_1(k_{1\rho r}\rho)J_0(k_{3\rho m}\rho) - \rho k_{1\rho r}J_0(k_{1\rho r}\rho)J_1(k_{3\rho m}\rho)]_g^b$$

$$BK_2 = \frac{N_0(k_{1\rho r}a)J_0(k_{3\rho m}b)}{\{k_{1\rho r}\}^2 - \{k_{3\rho m}\}^2}[\rho k_{3\rho m}J_1(k_{1\rho r}\rho)N_0(k_{3\rho m}\rho) - \rho k_{1\rho r}J_0(k_{1\rho r}\rho)N_1(k_{3\rho m}\rho)]_g^b$$

$$CK_2 = \frac{J_0(k_{1\rho r}a)N_0(k_{3\rho m}b)}{\{k_{3\rho m}\}^2 - \{k_{1\rho r}\}^2}[\rho k_{1\rho r}J_1(k_{3\rho m}\rho)N_0(k_{1\rho r}\rho) - \rho k_{3\rho m}J_0(k_{3\rho m}\rho)N_1(k_{1\rho r}\rho)]_g^b$$

$$DK_2 = \frac{J_0(k_{1\rho r}a)J_0(k_{3\rho m}b)}{\{k_{1\rho r}\}^2 - \{k_{3\rho m}\}^2}[\rho k_{3\rho m}N_1(k_{1\rho r}\rho)N_0(k_{3\rho m}\rho) - \rho k_{1\rho r}N_0(k_{1\rho r}\rho)N_1(k_{3\rho m}\rho)]_g^b$$

Appendix 2

MATLAB Subroutines used for this study

```
%% Call Forward Model for a specified frequency
clc
clear all
close all

gap= 0.8;           % gap thickness in mm
mx= 40;             % number of coaxial TM modes
nx= 50;             % number of circular waveguide TM modes
a= 2.9;             % coaxial inner conductor radius in [mm]
b= 19.055;          % coaxial outer conductor radius in [mm]
g= b-gap;
d= 50;              % Sample length in [mm]
L= 23.88;           % coaxial dielectric-filled line length in [mm]
L_air= 130;         % coaxial air-filled line length in [mm]
eps1= 5.1;          % coaxial dielectric-filled medium permittivity
eps3= 2;            % gap medium permittivity

%   conversion from mm to m
a= a*1e-3;
b= b*1e-3;
gap= gap*1e-3;
g= g*1e-3;
d= d*1e-3;
L= L*1e-3;
L_air= L_air*1e-3;

%   input Sample Properties in the sequence:
%   Frequency(Hz)   Dielectric Constant     Conductivity(S/m)

Data_e=[1000000.000 159.334   0.124];

%   input Reflection Coefficient data (S11) to comare with as:
%   Frequency(Hz)   S11_real     S11_imaginary

Data=[1000000.000 0.88   0.01];


Frequency1= Data_e(:,1);
e_real= Data_e(:,2);
cond_d= Data_e(:,3);

R=[mx nx];

w=2*pi*Frequency1;
eps0= double(8.854187817e-12);
```

```
mu0= double(4*pi*(1e-7));

eps2= complex(e_real,cond_d./(w.*eps0));    % Sample complex
permittivity


% computation of reflection coefficient and waveguide propagation
constant
for ff=1:length(Frequency1)

[R0(ff),kr2(ff,:)]=
forward_code(eps1,eps2(ff),eps3,R,Frequency1(ff),gap,L_air,a,b,d,L);

End
```

```
%% Forward modeling for coax-circular waveguide with gap effect

function [R0,kz2]=
forward_code(eps_coax,eps_s,eps_g,R,freq,gap,air_d,a_d,b_d,d_d,ld_d)
global a g b L d knc1r kng2n kng2m kng3n kng3m eps2 eps3


a= a_d;
b= b_d;
g= b-gap;
d= d_d;
L= ld_d;

coax_mode= round(R(1,1));
guide_mode= round(R(1,2));

eps1= eps_coax;
w=2*pi*freq;
eps0= double(8.854187817e-12);
mu0= double(4*pi*(1e-7));

eps2= eps_s;
eps3= eps_g;

% computation of propagation constants
krho1= comp_cutoff_coax(a,b,coax_mode);
[krho2, krho3]=
comp_cutoff_guide_complex2(g,b,freq,eps2,eps3,guide_mode);

kz2= zeros(1,length(krho2));
kz1= zeros(1,length(krho1));
Q_mr= zeros(length(krho2),length(krho1));
Nr= zeros(1,length(krho1));
knc1r= zeros(length(krho2),length(krho1));
kng2m= zeros(length(krho2),length(krho1));
kng3m= zeros(length(krho2),length(krho1));
kng2n= zeros(length(krho2),length(krho2));
kng3n= zeros(length(krho2),length(krho2));
M_mn= zeros(length(krho2),length(krho2));
```

```
Umn= zeros(length(krho2),length(krho2));


kz2= double(sqrt(w.*w.*mu0.*eps2.*eps0-krho2.*krho2));
kz1= double(sqrt(w.*w.*mu0.*eps1.*eps0-krho1.*krho1));

kz1(1,1)= double(w*sqrt(mu0*eps1*eps0));


for rr=1:length(krho2)
        knc1r(rr,:)= krho1;
end

for mm=2:length(krho1)

        kng2m(:,mm)=krho2';
        kng3m(:,mm)=krho3';
end



            AQ1= (1./(knc1r.*knc1r-
kng2m.*kng2m)).*(g.*kng2m.*bessely(0,knc1r.*a).*besselj(1,knc1r.*g).*be
sselj(0,kng2m.*g)-g.*knc1r.*bessely(0,knc1r.*a).*...
                besselj(0,knc1r.*g).*besselj(1,kng2m.*g)-
a.*kng2m.*besselj(1,knc1r.*a).*besselj(0,kng2m.*a).*bessely(0,knc1r.*a)
...
                -
g.*kng2m.*besselj(0,kng2m.*g).*bessely(1,knc1r.*g).*besselj(0,knc1r.*a)
+g.*knc1r.*besselj(1,kng2m.*g).*bessely(0,knc1r.*g).*besselj(0,knc1r.*a
)+...

a.*kng2m.*besselj(0,kng2m.*a).*bessely(1,knc1r.*a).*besselj(0,knc1r.*a)
);



            AQ2=
(besselj(1,kng2m.*g)./phi1n(kng3m,g,b,0,0)).*((bessely(0,knc1r.*a).*bes
sely(0,kng3m.*b)./(knc1r.*knc1r-kng3m.*kng3m)).*(...
                -
g.*kng3m.*besselj(1,knc1r.*g).*besselj(0,kng3m.*g)+g.*knc1r.*besselj(0,
knc1r.*g).*besselj(1,kng3m.*g))-
(bessely(0,knc1r.*a).*besselj(0,kng3m.*b)./(knc1r.*knc1r-
kng3m.*kng3m)).*(...
                -
g.*kng3m.*besselj(1,knc1r.*g).*bessely(0,kng3m.*g)+g.*knc1r.*besselj(0,
knc1r.*g).*bessely(1,kng3m.*g))-
(besselj(0,knc1r.*a).*bessely(0,kng3m.*b)./(kng3m.*kng3m-
knc1r.*knc1r)).*(...
                -
g.*knc1r.*besselj(1,kng3m.*g).*bessely(0,knc1r.*g)+g.*kng3m.*besselj(0,
kng3m.*g).*bessely(1,knc1r.*g))+(besselj(0,knc1r.*a).*besselj(0,kng3m.*
b)./(knc1r.*knc1r-kng3m.*kng3m)).*(...
```

```
                -
g.*kng3m.*bessely(1,knc1r.*g).*bessely(0,kng3m.*g)+g.*knc1r.*bessely(0,
knc1r.*g).*bessely(1,kng3m.*g)));



            Q_mr= AQ1+AQ2;
            Nr(1,:)=
((2./(pi.*pi.*knc1r(1,:).*knc1r(1,:))).*((besselj(0,knc1r(1,:).*a)./bes
selj(0,knc1r(1,:).*b)).^2-1));

            Q_mr(:,1)= (besselj(0,kng2m(:,2).*a)-
besselj(0,kng2m(:,2).*g))./kng2m(:,2)+besselj(1,kng2m(:,2).*g).*phi0n(k
ng3m(:,2),g,b,0,0)./phi1n(kng3m(:,2),g,b,0,0)./kng3m(:,2);
            Q_mr(1,:)= zeros(1,length(krho1));
            Q_mr= conj(Q_mr);
            Nr(1,1)= log(b/a);


 for km=2:length(krho2)
          kng2m(:,km)=krho2';
          kng3m(:,km)=krho3';

          kng2m(km,km)=1; % intentionally varied
          kng3m(km,km)=1;


end

for kn=2:length(krho2)
        kng2n(kn,:)=krho2;
        kng3n(kn,:)=krho3;

end

        kng2m=conj(kng2m);
        kng3m=conj(kng3m);


                M_mn_logic= diag(ones(1,length(krho2)),0);

                AF1=
0.5.*bessely(0,kng3n.*b).^2.*(b.*b.*besselj(0,kng3n.*b).^2+b.*b.*bessel
j(1,kng3n.*b).^2-2.*b.*besselj(0,kng3n.*b).*besselj(1,kng3n.*b)./kng3n-
...
                    g.*g.*besselj(0,kng3n.*g).^2-
g.*g.*besselj(1,kng3n.*g).^2+2.*g.*besselj(0,kng3n.*g).*besselj(1,kng3n
.*g)./kng3n);
                BF1=
bessely(0,kng3n.*b).*besselj(0,kng3n.*b).*(0.5*b.*b.*(besselj(0,kng3n.*
b).*bessely(0,kng3n.*b)+besselj(1,kng3n.*b).*bessely(1,kng3n.*b))-
b.*besselj(0,kng3n.*b).*bessely(1,kng3n.*b)./kng3n+...
```

```
                    g.*besselj(0,kng3n.*g).*bessely(1,kng3n.*g)./kng3n-
0.5*g.*g.*(besselj(0,kng3n.*g).*bessely(0,kng3n.*g)+besselj(1,kng3n.*g)
.*bessely(1,kng3n.*g)));
                CF1=
0.5.*besselj(0,kng3n.*b).^2.*(b.*b.*bessely(0,kng3n.*b).^2+b.*b.*bessel
y(1,kng3n.*b).^2-2.*b.*bessely(0,kng3n.*b).*bessely(1,kng3n.*b)./kng3n-
...
                    g.*g.*bessely(0,kng3n.*g).^2-
g.*g.*bessely(1,kng3n.*g).^2+2.*g.*bessely(0,kng3n.*g).*bessely(1,kng3n
.*g)./kng3n);

                M_mn_eq=
0.5.*(g.*g.*besselj(0,kng2n.*g).*besselj(0,kng2n.*g)+g.*g.*besselj(1,kn
g2n.*g).*besselj(1,kng2n.*g)-
2.*g.*besselj(1,kng2n.*g).*besselj(0,kng2n.*g)./kng2n)+(besselj(1,kng2n
.*g)./phi1n(kng3n,g,b,0,0)).^2.*...
                    (AF1-2.*BF1+CF1).*eps2./eps3;

                M_mn_1= M_mn_eq.*M_mn_logic;

                AF2=
(bessely(0,kng3m.*b).*bessely(0,kng3n.*b)./(kng3m.^2-kng3n.^2)).*(-
b.*kng3m.*besselj(0,kng3m.*b).*besselj(1,kng3n.*b)-
g.*kng3n.*besselj(1,kng3m.*g).*besselj(0,kng3n.*g)+...

g.*kng3m.*besselj(0,kng3m.*g).*besselj(1,kng3n.*g));
                BF2=
(besselj(0,kng3m.*b).*bessely(0,kng3n.*b)./(kng3n.^2-
kng3m.^2)).*(b.*kng3m.*besselj(1,kng3n.*b).*bessely(0,kng3m.*b)-
b.*kng3n.*besselj(0,kng3n.*b).*bessely(1,kng3m.*b)-...

g.*kng3m.*besselj(1,kng3n.*g).*bessely(0,kng3m.*g)+g.*kng3n.*besselj(0,
kng3n.*g).*bessely(1,kng3m.*g));
                CF2=
(bessely(0,kng3m.*b).*besselj(0,kng3n.*b)./(kng3m.^2-kng3n.^2)).*(-
g.*kng3n.*besselj(1,kng3m.*g).*bessely(0,kng3n.*g)+g.*kng3m.*besselj(0,
kng3m.*g).*bessely(1,kng3n.*b));
                DF2=
(besselj(0,kng3m.*b).*besselj(0,kng3n.*b)./(kng3m.^2-
kng3n.^2)).*(b.*kng3n.*bessely(1,kng3m.*b).*bessely(0,kng3n.*b)-
g.*kng3n.*bessely(1,kng3m.*g).*bessely(0,kng3n.*g)+...

g.*kng3m.*bessely(0,kng3m.*g).*bessely(1,kng3n.*g));
                I2=
(besselj(1,kng2m.*g).*besselj(1,kng2n.*g)./(phi1n(kng3m,g,b,0,0).*phi1n
(kng3n,g,b,0,0))).*(AF2-BF2-CF2+DF2);

                M_mn_neq= (g./(kng2m.*kng2m-
kng2n.*kng2n)).*(kng2n.*besselj(1,kng2m.*g).*besselj(0,kng2n.*g)-
kng2m.*besselj(0,kng2m.*g).*besselj(1,kng2n.*g))+I2.*eps2./eps3;


                M_mn_2= M_mn_neq.*not(M_mn_logic);

                M_mn= M_mn_1+M_mn_2;
```

```
                M_mn(1,:)= zeros(1,length(krho2));
                M_mn(:,1)= zeros(length(krho2),1);


%% To compute some constants and expression for the linear system

sum_Umn=zeros(guide_mode+1,guide_mode+1);

for kk=1:length(krho2)
    for ii=1:length(krho2)

            sum_Umn(kk,ii)=sum((kz1./Nr).*Q_mr(ii,:).*Q_mr(kk,:));

        gn= kz2(1,ii).*tan(kz2(1,ii)*d);

        Umn(kk,ii)= -1i*(eps1/eps2)*gn*M_mn(kk,ii)+sum_Umn(kk,ii);


    end
end

%%
% Solve the linear system for Dn

Dn= Umn\(2*Q_mr(:,1));

%%
% Solve for the reflection coefficient R0


R0_sum= 0;

for dd=2:length(Dn)

    R0_sum= R0_sum+Dn(dd,1)*Q_mr(dd,1);

end

R0= 1-(kz1(1,1).*R0_sum./Nr(1,1));

R0= R0.*exp(1i*2*kz1(1,1)*L).*exp(1i*2*w*sqrt(mu0*eps0)*air_d);


End
```

```
function [knc] = comp_cutoff_coax(a,b,nmode)


knc(1)=0.0d0;
x_delta=10;
x1=1;
f1=besselj(0,a*x1)*bessely(0,b*x1)-bessely(0,a*x1)*besselj(0,b*x1);
x2=1;
f2=besselj(0,a*x2)*bessely(0,b*x2)-bessely(0,a*x2)*besselj(0,b*x2);

for ii=1:nmode
  while ((f1*f2)> 0.0)
    x1=x2;
    f1=f2 ;
    x2=x2+x_delta;
    f2=besselj(0,a*x2)*bessely(0,b*x2)-bessely(0,a*x2)*besselj(0,b*x2);
  end

      options = optimset('Algorithm','levenberg-
marquardt','Display','off','TolFun',1e-10,'TolX',1e-10);
  x2 = fzero(@epsy0n,x2,options,a,b,0,0);
  knc(ii+1)=x2;
  x1=x2+x_delta;
  x2=x1;
  f1=besselj(0,a*x1)*bessely(0,b*x1)-bessely(0,a*x1)*besselj(0,b*x1);
  f2=f1;
end


end
```

```
function [kngc2,kngc3] = comp_cutoff_guide_complex2(g,b,f,e2,e3,nmode)


s= 1;

w= 2*pi*f;
mu0= double(4*pi*(1e-7));
eps0= double(8.854187817e-12);
x_delta=1;
kng2(1)=0.0d0+i*0.0;
kng3(1)=0.0d0i*0.0;
x1=1;
f1=TM_cutoff_loaded_guide(x1,g,b,f,e2,e3,s);
x2=1;
f2=TM_cutoff_loaded_guide(x2,g,b,f,e2,e3,s);

kngc2= zeros(1,nmode+1);
kngc3= zeros(1,nmode+1);



for ii=1:nmode
```

```
    if ii>1
        x_delta=20;
    end

  while kngc2(1,ii+1)==0



    while (f1.*f2> 0.0) % To detect zero-crossing

        x1=x2;
        f1=f2;
        x2=x2+x_delta;
        f2=TM_cutoff_loaded_guide(x2,g,b,f,e2,e3,s);

    end


    x0= [x2 0];
    options = optimset('Algorithm','levenberg-
marquardt','Display','off','TolFun',1e-10,'TolX',1e-10);
    x2=
fminunc(@TM_cutoff_loaded_guide_complex,x0,options,g,b,f,e2,e3,0);

    if x2(1,1)>real(kngc2(ii))+1
    kngc2(ii+1)= complex(x2(1,1),x2(1,2));
    kngc3(ii+1)=
sqrt(complex(x2(1,1),x2(1,2))*complex(x2(1,1),x2(1,2))-w.*w.*mu0.*(e2-
e3).*eps0);
    else
        x_delta=x_delta+20;
    end

  x1=x2(1,1)+x_delta;
  x2=x1;
  f1=TM_cutoff_loaded_guide(x1,g,b,f,e2,e3,s);
  f2=f1;

  end


end


end
```

```
function F = TM_cutoff_loaded_guide(x,g,b,f,e2,e3,select)

w= 2*pi.*f;
mu0= double(4*pi*(1e-7));
eps0= double(8.854187817e-12);

e2= double(e2);
```

```
e3= double(e3);

x= double(x);

k3= sqrt(x.*x-w.*w.*mu0.*eps0.*(e2-e3));

y= besselj(1,g.*x).*phi0n(k3,g,b,0,0).*e2.*k3-
e3.*phi1n(k3,g,b,0,0).*x.*besselj(0,g*x);


if select==1
    F= real(y)+imag(y);
else
    if select==2
        F= imag(y);
    else

F= abs(y);
end


end
```

```
function F = TM_cutoff_loaded_guide_complex(var,g,b,f,e2,e3,select)

w= 2*pi.*f;
mu0= double(4*pi*(1e-7));
eps0= double(8.854187817e-12);

x= double(var(1,1));
y= double(var(1,2));

k3= sqrt(complex(x,y).*complex(x,y)-w.*w.*mu0.*eps0.*(e2-e3));

y= besselj(1,g.*complex(x,y)).*phi0n(k3,g,b,0,0).*e2.*k3-
e3.*phi1n(k3,g,b,0,0).*complex(x,y).*besselj(0,g.*complex(x,y));


 if isfinite(var)
     y=y;
 else
     y= 0;
     'Singularity found at'
end

 if select==1
     F= real(y);

 else
     F= abs(y);
 end
end
```

```
%% Inversion Code

clc
clear all
close all

gap= 0.8;           % gap thickness in mm
mx= 40;             % number of coaxial TM modes
nx= 50;             % number of circular waveguide TM modes
R=[mx nx];
a= 2.9;             % coaxial inner conductor radius in [mm]
b= 19.055;          % coaxial outer conductor radius in [mm]
g= b-gap;
d= 50;              % Sample length in [mm]
L= 23.88;           % coaxial dielectric-filled line length in [mm]
L_air= 130;         % coaxial air-filled line length in [mm]
eps1= 5.1;          % coaxial dielectric-filled medium permittivity
eps3= 2;            % gap medium permittivity

%   conversion from mm to m
a= a*1e-3;
b= b*1e-3;
gap= gap*1e-3;
g= g*1e-3;
d= d*1e-3;
L= L*1e-3;
L_air= L_air*1e-3;

%% Data input

Data= [1000000.0000000000   0.8972670391    0.8970801919    -
0.0183103469];

epsi_dd=[     1000000.000 159.334   0.124        0.0000072170];


Frequency1= Data(:,1);
gamain_real= Data(:,3);
gamain_imag= Data(:,4);


for ff=1:length(Frequency1);

    if ff==1
        x(1)= 100;      % set initial guess value for permittivity
        x(2)= 0.1;      % set initial guess value for conductivity
    else
        x(1)= perm(ff-1,1);     % use previous inversion result for
next guess
        x(2)= cond(ff-1,1);
    end


w= 2*pi*Frequency1(ff);
```

```
mu0= double(4*pi*(1e-7));
eps0= double(8.854187817e-12);


x0= double([x(1) x(2)]);

% Initialize optimization process to find best fit for measured S11
OPTIONS = optimset('Algorithm','levenberg-
marquardt','Display','off','MaxIter',100,'TolFun',1e-10,'TolX',1e-5);
[x,FVAL]=fminsearch(@Cost_mingama,x0,OPTIONS,eps1,eps3,R,Frequency1(ff)
,gap,L_air,a,b,d,L,gamain_real(ff),gamain_imag(ff));

perm(ff,1)= x(1)    % inverted sample real permittivity
cond(ff,1)= x(2)    % inverted sample conductivity

figure(10)
semilogx(Frequency1(1:length(perm),1),perm,'b',Frequency1(1:length(perm
),1),epsi_dd(1:length(perm),2),'xr'), axis([1e6 1e9 1 200])

figure(20)
semilogx(Frequency1(1:length(perm),1),cond,'b',Frequency1(1:length(perm
),1),epsi_dd(1:length(perm),3),'xr'), axis([1e6 1e9 0 0.5])

end
```

```
function f =
Cost_mingama(x,eps1,eps3,R,freq,gap,L_air,a,b,d,L,gama_r,gama_i)
%minimize reflection coefficient



%compute gama_x
%to be sure x is always real values
x(1) = double(real(x(1)));
x(2) = double(real(x(2)));

w=2*pi*freq;
eps0= double(8.854187817e-12);
epss= complex(x(1),x(2)./(w.*eps0));

[gamax,kz2] = forward_code(eps1,epss,eps3,R,freq,gap,L_air,a,b,d,L);

%construct cost function
%assume gama_in = a + i*b
%       gama    = a1+ i*b1
% cost function choose to be (a-a1)^2 + (b-b1)^2
ain = gama_r;
bin = gama_i;
a1m = real(gamax);
b1m = imag(-gamax);
f = 0.5*((ain-a1m)*(ain-a1m) + (bin-b1m)*(bin-b1m));

end
```

```
function y= phi1n(r,g,b,kn,select)

if select==1

y= besselj(1,kn.*r).*bessely(0,kn.*b)-
besselj(0,kn.*b).*bessely(1,kn.*r);

else
     y= besselj(1,r.*g).*bessely(0,r.*b)-
besselj(0,r.*b).*bessely(1,r.*g);

end
```

```
function y= phic_1n1m_2_mod(r)

global g b kng2n kng2m kng3n kng3m eps2 eps3

y=
r.*phic_1n(r,g,b,kng2n,kng3n,2).*phic_1n(r,g,b,kng2m,kng3m,2).*eps2./ep
s3;

end
```

```
function y= phi0n(r,g,b,kn,select)

if select==1
y= besselj(0,kn.*r).*bessely(0,kn.*b)-
besselj(0,kn.*b).*bessely(0,kn.*r);

else
    y= besselj(0,r.*g).*bessely(0,r.*b)-
besselj(0,r.*b).*bessely(0,r.*g);
end
```

```
function y= phic_1n1m_1(r)

global g b kng2n kng2m kng3n kng3m

y= r.*phic_1n(r,g,b,kng2n,kng3n,1).*phic_1n(r,g,b,kng2m,kng3m,1);

end
```

```
function y= phic_1n1m_2(r)

global g b kng2n kng2m kng3n kng3m

y= r.*phic_1n(r,g,b,kng2n,kng3n,2).*phic_1n(r,g,b,kng2m,kng3m,2);


end
```

```
function y= phic_1m1m_1(r)

global g b kng2n kng2m kng3n kng3m

y= r.*phic_1n(r,g,b,kng2m,kng3m,1).*phic_1n(r,g,b,kng2m,kng3m,1);

end
```

```
function y= phic_1m1m_2(r)

global g b kng2n kng2m kng3n kng3m

y= r.*(phic_1n(r,g,b,kng2m,kng3m,2)).*(phic_1n(r,g,b,kng2m,kng3m,2));

end
```

```
function y= phic_1n(r,g,b,kng2,kng3,select)

if select==1
y= besselj(1,r.*kng2);

else
    if select==2
        c= besselj(1,kng2.*g)./phi1n(kng3,g,b,0,0);
    y= c.*phi1n(r,g,b,kng3,1);

    end
end
```

```
function y= epsy_phic_101m_2(r)

global a g b kng2m kng3m

y= phic_1n(r,g,b,kng2m,kng3m,2);

end
```

```
function y= epsy_phic_101m_1(r)

global g b kng2m kng3m

y= phic_1n(r,g,b,kng2m,kng3m,1);

end
```

```
function y= epsy_phic_1r1m_2(r)
global a g b knc1r kng2m kng3m

y= r.*epsy1n(r,a,b,knc1r,1).*phic_1n(r,g,b,kng2m,kng3m,2);

end
```

```
function y= epsy_phic_1r1m_1(r)

global a g b knc1r kng2m kng3m

y= r.*epsy1n(r,a,b,knc1r,1).*phic_1n(r,g,b,kng2m,kng3m,1);

end
```

```
function y= epsy_phic_101m(r,g,b,kng2m,kng3m,select)

y= phic_1n(r,g,b,kng2m,kng3m,select);

end
```

```
function y= epsy_phic_1r1m(r,a,g,b,knc1r,kng2m,kng3m,select)

y= r.*epsy1n(r,a,b,knc1r,1).*phic_1n(r,g,b,kng2m,kng3m,select);

end
```

```
function y= phic_1n1m(r,g,b,kng2n,kng2m,kng3n,kng3m,select)

y=
r.*phic_1n(r,g,b,kng2n,kng3n,select).*phic_1n(r,g,b,kng2m,kng3m,select)

end
```

```
function y= phic_0n(r,g,b,kng2,kng3,select)

if select==1
y= besselj(0,kng2.*r);

else
    if select==2

        c= besselj(0,kng2.*g)./phi0n(kng3,g,b,0,0);
    y= c.*phi0n(r,g,b,kng3,1);

    end
end
```